NASA Contractor Report 4575

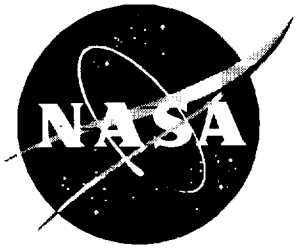

Nonaqueous Slip Casting of $YBa_2Cu_3O_{7-x}$ Superconductive Ceramics

Matthew W. Hooker and Theodore D. Taylor
Clemson University • Clemson, South Carolina

National Aeronautics and Space Administration
Langley Research Center • Hampton, Virginia 23681-0001

Prepared for Langley Research Center
under Grant NGT-50548

March 1994

ABSTRACT

This study investigates the slip casting of $YBa_2Cu_3O_{7-x}$ powders using nonaqueous carrier liquids and fired ceramic molds. The parameters of the process examined here include (1) the rheological properties of $YBa_2Cu_3O_{7-x}$ powder dispersed in various solvent/dispersant systems, (2) the combination of nonaqueous slips with fired ceramic molds to form the superconductive ceramics, (3) the process-property relationships using a four-factor factorial experiment, and (4) the applicability of magnetic fields to align the $YBa_2Cu_3O_{7-x}$ grains during the casting process.

The solvent/dispersant system found to be most suitable for slip casting consisted of acetone and Menhaden fish oil. $YBa_2Cu_3O_{7-x}$ powder dispersed in this system possessed a viscosity minimum of approximately 85 cps at dispersant concentrations of 0.75 to 1.75 volume percent. The casting of these slips into fired ceramic molds resulted in the successful forming of $YBa_2Cu_3O_{7-x}$ ceramics which, after firing to 940°C, exhibited a superconductive transition at 90 K.

The results of the factorial experiment indicate that the critical process parameters are the particle size distribution, the sintering temperature, and the interaction of these variables. Densities on the order of 90% of theoretical density and critical current densities ranging from 75-110 A/cm^2 were obtained when near-ideal particle size distributions were employed and the castings were fired at 935°C.

The application of a magnetic field to this forming process yielded c-axis oriented ceramics as determined by both X-ray diffraction and scanning electron microscopy. However, no corresponding alignment of the current carrying ab planes were observed. As a result, the application of a magnetic field did not enhance the critical current density of the superconductor.

ACKNOWLEDGEMENTS

This research was conducted at NASA-Langley Research Center through the sponsorship of the NASA Graduate Student Researchers Program (Grant Number NGT-50548). Both the opportunity to perform this work at Langley Research Center and NASA's financial support of this endeavor are appreciated.

The authors would also like to express their gratitude to Pete Vasquez and Ralph Stephens of NASA-LaRC and Drs. Raouf Selim and Randall Caton of Christopher Newport University for their assistance in completing this work.

TABLE OF CONTENTS

Table of Contents (Continued)

LIST OF TABLES

LIST OF FIGURES

List of Figures (Continued)

List of Figures (Continued)

INTRODUCTION

The discovery of superconductivity in ceramics above liquid nitrogen temperatures (77 K) has created renewed interest in the applicability of these unique materials [1-3]. However, the fabrication of these ceramics has been limited by their anisotropic nature and chemical instability in water [4-9].

Some traditional ceramic forming processes (e.g., extrusion and pressing) have been employed to form these materials by substituting organic carrier liquids for water [10-13]. However, slip casting these materials using organic carrier liquids has not proven successful because the plaster of Paris molds typically used in slip casting operations are incompatible with the organic liquids [14].

This study investigates the slip casting of $YBa_2Cu_3O_{7-x}$ superconducting ceramics using organic carrier liquids in combination with molds prepared by a lost wax process [15]. After selecting suitable solvent/dispersant systems for the preparation of stable non-aqueous slips, emphasis was placed on optimizing the critical process parameters. This project also investigated the influence of magnetic fields, applied during the casting process, on the critical current density of the superconductors.

STATEMENT OF EXPERIMENTAL OBJECTIVES

The purpose of this investigation is to demonstrate the feasibility of forming high temperature ceramic superconductors (e.g., $YBa_2Cu_3O_{7-x}$) into unique configurations using a non-aqueous slip casting process. In this process, molds prepared by a lost-wax technique are employed instead of plaster of Paris molds which are incompatible with the organic carrier liquids employed in this work.

This research is divided into three phases. First, the viscosity and stability of various solvent/dispersant systems will be evaluated in order to prepare stable, non-aqueous slips. The second phase of the research will identify the critical process parameters (e.g., particle size distribution, sintering temperature, and silver additions) necessary to produce high quality ceramics. The properties which will be used to determine the quality of the cast ceramics are density, critical current density (J_c), dry shrinkage, and fired shrinkage. The final phase of this work will demonstrate the applicability of magnetic alignment to the slip casting process as a means of overcoming the anisotropic nature of the $YBa_2Cu_3O_{7-x}$ ceramics and thus enhancing the critical current density of the cast superconductors.

REVIEW OF LITERATURE:

SUPERCONDUCTIVITY

Introduction

Before the liquification of helium in 1908 by H.K. Onnes, researchers were unable to study the electrical properties of materials near absolute zero. In 1911, while studying the resistivity of metals at low temperatures, Onnes discovered that the resistivity of mercury dropped abruptly to zero at 4.2 K. This phenomenon of zero resistance was referred to as superconductivity, and the temperature at which this transition occured became known as the superconductive transition temperature, T_c [16-19].

Early in his research with superconductivity, Onnes found that the superconductive state could be reversibly quenched by passing currents above a certain level through the specimen. The loss of superconductivity was attributed to the presence of the magnetic field produced by the applied current. Thus, the superconductive state would only exist if the induced magnetic field remained below some critical magnetic field, H_c. This value has a quantity which varies from a maximum at absolute zero to a minimum at the critical temperature. The relationship between temperature and magnetic field strength is shown in Figure 1.

In addition to the studies of zero resistance, Meissner [20] began to examine the unique magnetic properties of superconductors in 1933. He found that in the presence of a

weak magnetic field, a bulk superconductor behaves as a perfect diamagnet, with no magnetic induction in the interior of the material. The expulsion of magnetic flux from the interior of a superconductor became known as the Meissner effect and is shown schematically in Figure 2.

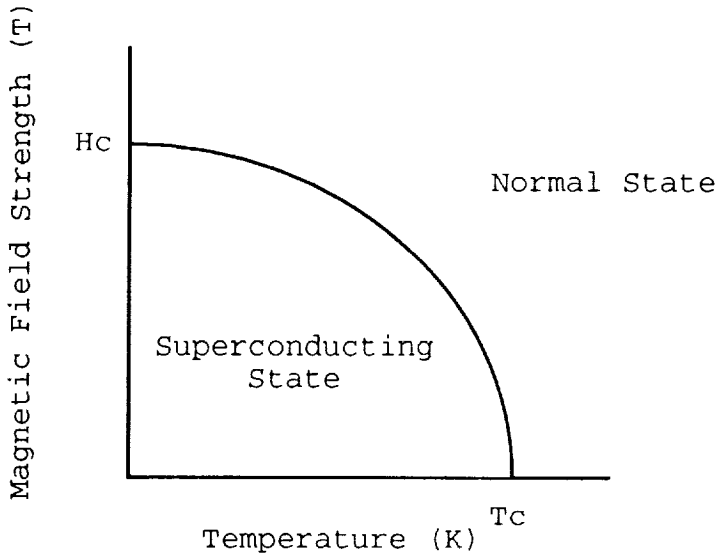

Figure 1. Relationship between temperature and critical field [17].

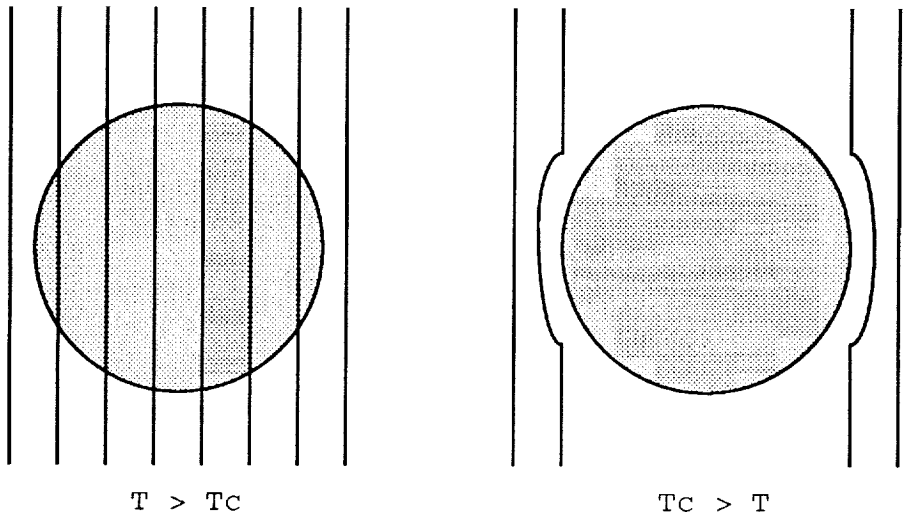

Figure 2. Schematic representation of the Meissner effect [17].

Type I and Type II Superconductivity

About half of the known metals as well as several metal alloys have been found to be superconducting below some critical temperature. Whereas the mechanism of electronic transport is the same in all metallic superconductors, the magnetic properties of superconductors fall into two distinct categories. These two behaviors became known as Type I and Type II superconductivity.

Type I superconductors exhibit an abrupt change from the superconducting state to the normal state above H_c, with perfect diamagnetism below H_c. As seen by Onnes, this transformation to the normal state occurs at relatively low applied magnetic field strengths, limiting the current that can be passed through the materials and thus restricting their applicability.

Whereas Type I superconductors become normal at H_c, Type II superconductors have two critical magnetic field levels, namely H_{c1} and H_{c2}. Below H_{c1}, Type II superconductors possess properties similar to those of Type I superconductors. When an applied magnetic field is above H_{c1} and below H_{c2}, Type II superconductors are in what is referred to as a vortex state.

From a practical point of view, the most important aspect of the vortex state is flux pinning. As a magnetic field approaches a Type II superconductor, the magnetic flux lines are trapped or pinned by randomly distributed, normal (non-superconducting) regions in the material. The normal sites which serve as flux pinning centers are typically defects in the

material such as impurities, dislocations, and grain boundaries. The restriction of flux motion is important in increasing both the current carrying capacity and the levitative forces of the superconductor. Some examples of Type I and Type II superconductors and their critical temperatures and magnetic fields are given in Table 1. Additionally, a graphic illustration of the differences between Type I and Type II superconductors is shown in Figure 3 [16-19].

BCS Theory

After the discovery of superconductivity, several theories describing the phenomenon of zero resistance were proposed, but no widely accepted theory existed until 1957. In that year, John Bardeen, Leon Cooper, and Robert Schrieffer proposed that superconductivity was based on electron-phonon interactions, and their theory became known as the BCS theory [21].

The basic principle described by the BCS theory is that below T_c, electrons travel in pairs (referred to as "Cooper pairs") [22]. At very low temperatures, electrons are at their lowest energy states, as are the atoms that comprise the crystal lattice of the superconductor. Under these conditions, electrons of opposite spin directions may pair and travel through the crystal lattice unhindered by lattice vibrations. At higher temperatures, the crystal lattice vibrations increase, increasing the probability of collisions between the electrons and the lattice atoms which results in the break-up

Table 1. Critical temperatures (T_c) and magnetic fields (H_c) for selected Type I and Type II superconductors [18].

Superconductor	T_c in Zero Field (K)	Critical Magnetic Field at 0°K (Tesla)
Type I		
Al	1.19	0.0102
In	3.4	0.0285
Sn	3.72	0.0305
Ta	4.48	0.805
La	6.1	0.160
Pb	7.19	0.0803
Type II		
Ta_3Sn	8.35	24.5 (H_{c2})
NbTi	9.6	12.2 (H_{c2})
V_3Ga	16.5	35 (H_{c2})
Nb_3Al	17.1	25 (H_{c2})
Nb_3Sn	18.1	25 (H_{c2})
Nb_3Ge	23.2	38 (H_{c2})

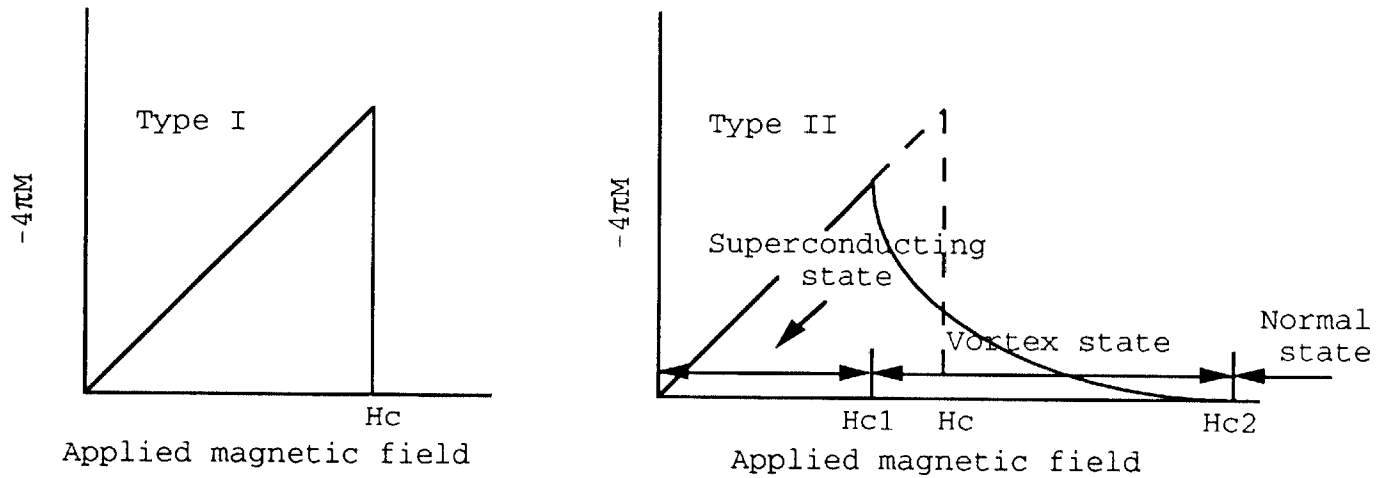

Figure 3. Magnetic properties of Type I and Type II superconductors [16-19].

of the electron pairs. To compensate for lattice vibrations, a theoretical limit of 30 K for T_c was included in the BCS theory. Although superconductors with T_c's greater than 30 K have since been discovered, the basic principles of the BCS theory are still considered to be valid.

Discovery of High Temperature Superconductivity

In 1986, Georg Bednorz and Alex Muller of IBM's Zurich Research laboratory discovered superconductivity at 30 K in La-Ba-Cu-O [23]. Before their discovery, the highest T_c recorded was 23 K in Nb_3Sn.

After this discovery, many scientists began substituting elements for Ba in the La-Ba-Cu-O compound in an effort to further increase T_c. However, no real breakthroughs were made until researchers at the University of Alabama at Huntsville and the University of Houston collaborated on the substitution Y for La resulting in the obtainment of superconductivity at 93 K in $YBa_2Cu_3O_{7-x}$ [1].

Shortly thereafter, two more families of high temperature superconductors were discovered, namely Bi-Sr-Ca-Cu-O [2] and Tl-Ba-Ca-Cu-O [3]. Both of these families have members with superconducting transition temperatures above 100 K. Table 2 provides a listing of the various high temperature superconductors and their transition temperatures.

Table 2. Superconductive compounds and their transition temperatures.

Compound	T_c (K)
$YBa_2Cu_3O_{7-x}$	93
$Bi_2Sr_2Ca_1Cu_2O_x$	85
$BiSrCaCu_2O_x$	105
$Bi_2Sr_2Ca_2Cu_3O_x$	114
$Tl_2Ba_2CuO_{6+x}$	80
$Tl_2Ba_2CaCu_2O_{8+x}$	110
$Tl_2Ba_2Ca_2Cu_3O_x$	125

Properties of High Tc Superconductors

All of the copper oxide superconductors discovered to date possess perovskite crystal structures. In each compound, the copper and oxygen atoms occupy lattice sites, producing the Cu-O chains thought to be responsible for superconductivity in these materials. The Cu-O planes are visible in the $YBa_2Cu_3O_{7-x}$ unit cell shown in Figure 4 [4].

The unique characteristic of this compound with regard to the other superconductive copper oxide compounds is the oxygen dependency. As the $YBa_2Cu_3O_{7-x}$ compound is heated, oxygen is lost resulting in the formation of the oxygen deficient, tetragonal phase ($YBa_2Cu_3O_{6.3}$). Upon cooling in oxygen (or air), the compound picks up oxygen and reverts back to the orthorhombic (superconducting) phase which exists when $0<x<0.7$ [24].

Additionally, the crystal structure of $YBa_2Cu_3O_{7-x}$ is highly anisotropic, with higher current transport properties along the ab plane than along the c plane. Therefore, to produce superconductive ceramics with an enhanced critical current density (Jc), some means of orienting the grains must be employed [10,11,13].

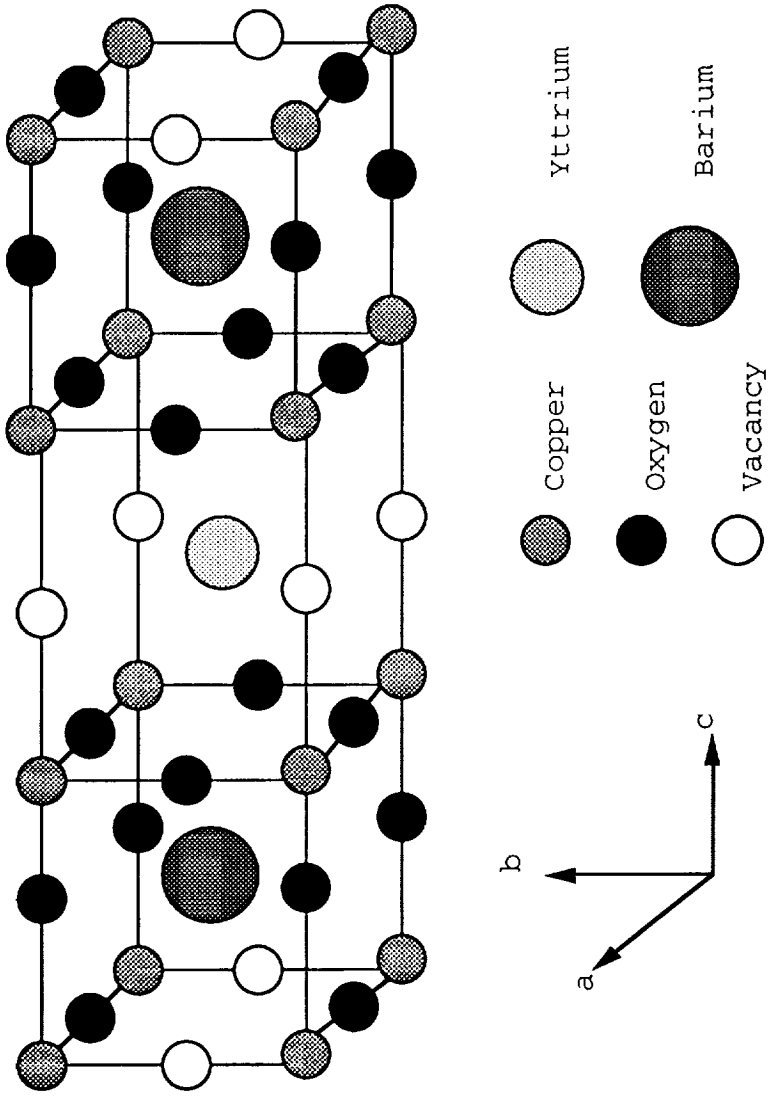

Figure 4. Idealized $YBa_2Cu_3O_{7-x}$ crystal structure [4].

Enhancement of Current Transport in Y-Ba-Cu-O

Typically, sintered samples of $YBa_2Cu_3O_{7-x}$ have critical current densities below 100 A/cm^2. These relatively low values are attributed to the anisotropic nature of the materials and to weak links resulting from grain boundaries present in the ceramics. Higher current densities are necessary for many of the proposed applications of high T_c materials [25-26]. Several approaches have been taken to increase the current carrying ability of these ceramics.

The first significant enhancement of the current transport properties in bulk $YBa_2Cu_3O_{7-x}$ was accomplished by Peters et al [27]. $YBa_2Cu_3O_{7-x}$ samples were doped with silver in an effort to eliminate the effects of the weak intergranular coupling by integrating a conductive material into the grain boundaries. Current densities between 125 and 350 A/cm^2 have been reported for Ag-doped $YBa_2Cu_3O_{7-x}$ [28-31].

In addition to silver dopants, two high temperature processes have been developed which produce samples with current densities greater than 1000 A/cm^2. The first of these techniques is referred to as melt texturing. In this process, small samples (0.1-1 x 0.5-2 x 30 mm) of $YBa_2Cu_3O_{7-x}$ are heated to approximatly 1040°C and then cooled through a temperature gradient at a rate of approximately 5°C/mm. By cooling the melted material through a temperature gradient, the specimen recrystallizes in one direction, resulting in a grain-oriented microstructure. Current densities greater than 2500 A/cm^2

have been reported for melt textured specimens in the technical literature [32-38].

The one limitation of this procedure, however, is that only the grains on the surface of the sample are oriented because the interior of the sample does not see the effect of the thermal gradients. Thus, only very small samples have been produced [39].

More recently, bulk specimens of $YBa_2Cu_3O_{7-x}$ have been produced by a melt-process melt-growth (MPMG) technique. In this procedure, $YBa_2Cu_3O_{7-x}$ with excess yttrium is heated to 1400°C and the resulting liquid is then quenched to room temperature. The amorphous material is then ground, pelletized, and heated to 1100°C and cooled slowly to 900°C to recrystallize the superconducting phase. The material is then annealed in oxygen to produce the superconducting phase [40-42].

Superconducting ceramics produced by this technique have excellent levitative properties. The enhanced levitative properties of these materials are attributed to the excess yttrium which serves as randomly distributed flux pinning sites [43-46]. Due to the presence of flux pinning sites in these materials, critical current densities inferred from magnetic measurements have been reported to be as high as 30,000 A/cm^2 [44]. Although these materials have superior levitative properties, direct current transport measurements of only 1000 A/cm^2 have been measured. This value is lower than expected because of residual amorphous phases present in the grain boundaries [46].

In addition to thermal processes, grain-oriented specimens of $YBa_2Cu_3O_{7-x}$ have also been produced by magnetic alignment of the superconducting grains. In these studies, $YBa_2Cu_3O_{7-x}$ powder is dispersed in an organic solvent in a crucible and placed in a magnetic field. The powder is oriented in the liquid with the ab plane perpendicular to the applied field. Once the oriented powders have settled out of the liquid, the solvent is allowed to evaporate and the powder is fired to 950°C while in the crucible. The resulting compacts possess a high degree of grain orientation according to X-ray diffraction studies and have critical current densities above 200 A/cm^2. Typically, magnetic field strengths of at least 0.5 Tesla are needed to orient the superconducting material [47-55].

The various methods of increasing the current carrying capacity of $YBa_2Cu_3O_{7-x}$ ceramics and the resulting current densities of the materials produced by each technique are summarized in Table 3.

Applications of Superconductivity

Before the discovery of high temperature superconductors, the usefulness of superconductors was limited by both the complexity and size of the liquid helium refrigeration systems required to cool the materials below their superconducting transition temperatures. The recent discovery of superconductors with transition temperatures greater than 77 K has made many superconductive devices more feasible as liquid

Table 3. Critical current density (A/cm^2) values obtained through texturing procedures.

Process	J_c (A/cm^2)	Reference
Sintered $YBa_2Cu_3O_{7-x}$	40	Malik et.al.[32]
Ag-doping	250-350	Peters et.al.[27]
	125-225	Malik et.al.[32]
Melt Texturing	3100-7400	Jin et.al.[33-34]
	8500	McGinn et.al.[38]
MPMG	1000	Chen et.al.[46]
Magnetic Alignment	440	Chen et.al.[52]
	200	Tkaczyk et.al.[54]

nitrogen refrigeration systems are less complex than liquid helium systems [56].

As refrigeration becomes a less critical issue, the use of superconductors in electronics has become more practical. Several high Tc devices have been examined for potential application including computers, switches, microwave devices, and antennas. In each instance, superconductivity provides an improvement over existing non-superconducting devices [57-59].

Whereas electronics appears to be an obvious application of the new high Tc materials, magnetic devices are also under development. One such device is a superconductive magnetic bearing. Conventional magnetic bearings use electromagnetically controlled components to isolate the rotating parts. Conversely, the use of superconductive bearings eliminates the need for an additional power supply by employing the Meissner effect to separate the rotating elements, thus reducing the power requirements and weight of the system [60-61]. Other areas in which the Meissner effect could be used include vibration damping [62] and magnetic shielding [63]. A listing of the potential applications of high T_c superconductors and the advantage of such systems over existing technology is given in Table 4.

Fabrication of High Tc Devices

Many of the proposed electronic applications require the superconductor to possess high current densities. To produce these devices, several thin film deposition techniques (e.g.,

Table 4. Applications and advantages of high temperature superconductivity.

Application	Advantage of High Tc Materials
Electronic Devices	
Computers	increase speed
Electronic switches	increase speed
Microwave electronics	low RF surface resistance
Antennas	decrease size required
SQUIDs	increase Tc
Bolometers	potential for passive cooling
Energy storage	increase Tc, no loss storage
Magnetic Devices	
Magnetic bearings	contactless rotation
Vibration damping	Meissner effect to damp vibrations
Magnetic shielding	passive device at 77 K
High field magnets	increase Tc; requires improved Jc for application

sputtering, laser ablation, electron beam evaporation, etc.) have been successfully employed to grow highly oriented superconducting films on single crystal substrates, possessing current densities on the order of 10^5 to 10^6 A/cm^2. A review of the techniques employed to produce superconducting thin films is given by Leskala et al [64].

Additionally, thick film superconductors have been deposited onto polycrystalline substrates using a screen-printing technique. These thick films have current density values similar to those of other bulk superconductive ceramics and are acceptable for some electronic applications [65-66].

In addition to film deposition, bulk superconductive ceramics such as wires, coils, and cylinders have been produced by tape casting, extrusion, and isostatic pressing. Each of these techniques results in the production of randomly oriented, polycrystalline materials with relatively low current densities, as no texturing technique is used in conjunction with the forming technique [10-13]. The concept of using magnetic fields to align the superconductive grains during the forming of bulk ceramics has been proposed [13]; however, researchers have thus far been unable to demonstrate the combination of a ceramic forming process and magnetic texturing [67].

Summary

Since its discovery, several applications of superconductivity have been proposed. However, due to the cost and complexity of liquid helium refrigeration units, most of these applications were impractical. The recent discovery of high

temperature superconductors has created renewed interest in many of these applications, as liquid nitrogen refrigeration systems can replace the more complex liquid helium systems.

High temperature superconductors have been fabricated by both thin film and powder processing techniques. Processing problems, however, have hindered the commercialization of these materials. As the development of more reliable processing techniques proceeds, these materials may be integrated into a variety of systems.

REVIEW OF LITERATURE:

SLIP CASTING

Introduction

One potential means of forming ceramic superconductors into desired configurations is that of slip casting [13,67]. Slip casting is a ceramic forming process employed to produce a wide variety of ceramic products including such traditional ceramics as whitewares and sanitarywares as well as high performance ceramics such as Si_3N_4 automobile engine components [68]. The basic steps of the slip casting process are as follows [68-71]:

1. A stable suspension of ceramic powders (or slip) is prepared.
2. The slip is poured into a porous mold which absorbs the liquid, thus producing a ceramic in the shape of the mold.
3. After a wall thickness has developed, the excess slip is either poured off to produce a hollow shape, or left in place to make a solid shape.
4. The cast ceramic is dried.
5. The cast part is fired to yield the final product.

A schematic of this process is shown in Figure 5.

In initiating a slip casting process, the selection of a carrier liquid/dispersant system and a suitable mold must be addressed. Typically, water is used as the carrier liquid, and slip casting is performed in plaster of Paris molds. In some instances, however, the material to be cast is unstable in water (e.g., $YBa_2Cu_3O_{7-x}$ [5-9]) and an alternative carrier

(a) Drain casting

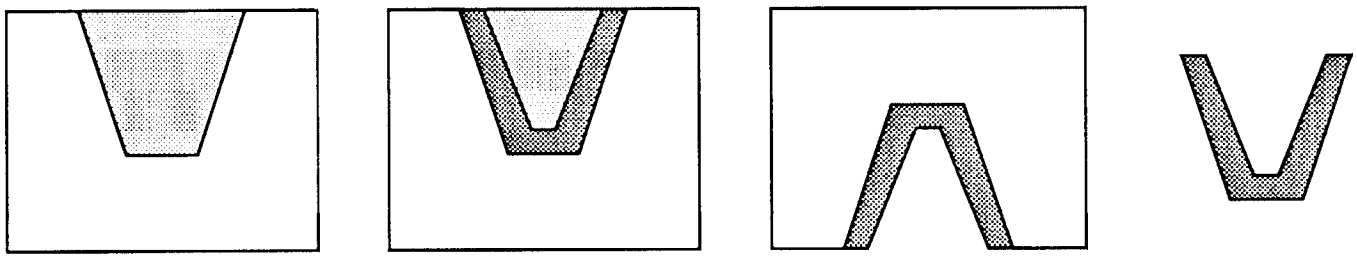

(b) Solid casting

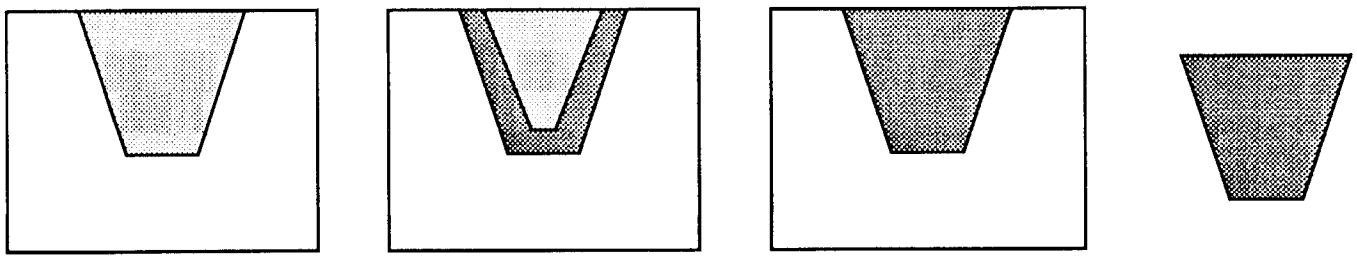

Figure 5. Schematic of the slip casting process for the production of (a) thin walled ceramics and (b) solid ceramics.

liquid must be selected. In these instances, the mold material must also be changed, as non-aqueous liquids are incompatible with plaster of Paris molds [14,67].

Dispersing Ceramic Powders in Liquid Media

To produce stable suspensions of ceramic powders for slip casting, chemical additives, referred to as deflocculants are employed. Deflocculants adsorb onto the surfaces of ceramic particulates, keeping them in suspension by electrostatic repulsion and/or steric hindrance. Both of these dispersing mechanisms prevent the close approach of the particles, thus imparting stability to the suspension [72-76].

Deflocculants used in aqueous systems typically possess a hydrocarbon portion and a polar or ionic portion. The hydrocarbon portion, which may be linear or branched, interacts only very weakly with water molecules and goes to the surface of the ceramic particulates to avoid the aqueous environment. Because of the hydrocarbon's aversion to water, this part of the molecule is referred to as hydrophobic (i.e., "water hating"). The polar or ionic portion of the molecule interacts strongly with the water present and is said to be hydrophilic (i.e., "water liking"). The ionic component of the dispersant is responsible for preventing the close approach of similarly charged particles in aqueous systems [68,72-76].

Steric Stabilization

In some instances, as with $YBa_2Cu_3O_{7-x}$, the ceramic powder to be dispersed is unstable in water. Therefore, to prepare suspensions of such powders, a non-aqueous liquid must be used. Since most organic liquids have low dielectric constants, electrostatic repulsion can not be relied upon to disperse the powders, and another mechanism must be employed. In systems where the DLVO theory is not applicable, steric stabilization is utilized [68,72-78].

Unlike electrostatic repulsion, the stabilization of a suspension by steric hindrance does not require ionic dispersants. Instead, block co-polymers possessing a lyophobic (i.e., solvent "hating") head and a lyophilic (i.e., solvent "liking') tail are employed. The lyophobic head attaches strongly to the surface of the particles present, and the lyophilic tail is solvated into the continuous liquid phase [72-78].

As two surfaces, each covered by a layer of soluble polymer chains, approach each other to within a distance less than the combined thickness of the adsorbed layers, an interaction between the polymer layers will occur. This interaction is the source of steric stabilization, and results in the development of a repulsive force between the two approaching particulates as shown in Figure 6 [74].

As shown in Figure 6, when the adsorbed layers overlap, the chemical potential of the solvent ($\mu_i ß$) is lower inside the overlap region (dV) than in areas outside ($\mu_i \alpha$) of it.

Because of the resulting difference in chemical potential, the solvent molecules in the continuous phase will tend to diffuse into the overlap region, forcing the approaching particles away from each other.

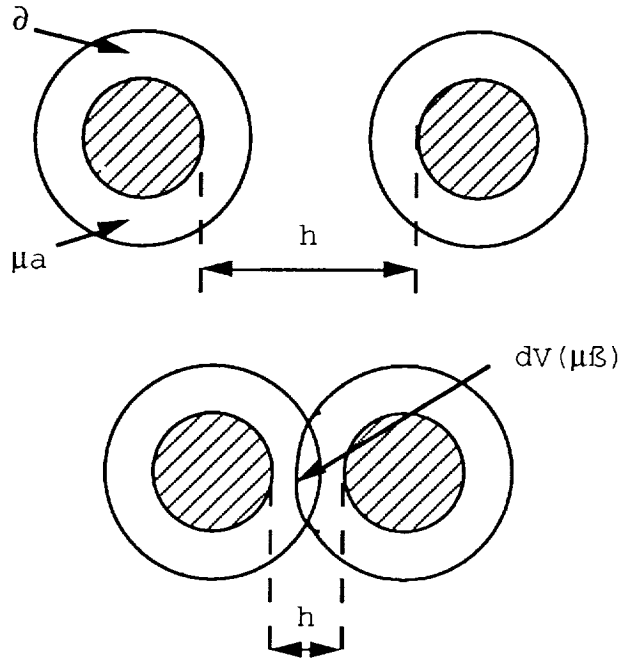

Figure 6. Schematic representation of adsorbed layers in a sterically stabilized system [74].

Dispersants for Steric Stabilization

Non-ionic compounds such as oleic acid, stearic acid, and Menhaden fish oil have been employed to disperse powders in non-aqueous media [79-82]. Steric stabilizers possess definite lyophobic head and lyophilic tail groups. For the organic dispersants mentioned, the -COOH radicals attach to the surface of the ceramic powder, and the polymer chain is dissolved into the continuous phase [68,77]. In addition to -COOH

radicals, other radicals such as -OH and $-C_6H_6$ groups may be employed as the lyophobic portion of a dispersant [77].

Polymeric dispersants possessing charged chemical radicals such as phosphates and cationic species (e.g., Na^+) have also been employed to disperse ceramic powders in liquids with low dielectric constants [80-88]. The types of dispersants are thought to keep particulates in suspension by a combination of steric and electrostatic forces as described by Fowkes [89]. Table 5 provides a list of some solvent/dispersant systems used to disperse ceramic powders in organic liquids.

Molds for Slip Casting

Once a stable slip has been developed, the next step in the casting process is mold selection. In most slip casting operations, plaster of Paris molds are used. In some instances, however, the material to be slip cast is not stable in water, and an alternative carrier liquid must be selected [71]. Attempts to disperse these ceramic powders in non-aqueous media and cast the resulting suspensions in plaster of Paris molds have been unsuccessful. In these instances, the researchers found it impossible to remove the cast body from the mold [71]. Greenaway [14] successfully cast MgO in solvent extraction thimbles using organic carrier liquids, but the use of the thimbles as molds restricts the selection of shapes to be produced.

Other alternatives to plaster of Paris molds do exist, although none have been used in combination with non-aqueous

Table 5. Examples of ceramic powders dispersed in organic liquids.

Ceramic Powder	Liquid Medium	Dispersant	Reference
Al_2O_3	p-xylene	Na AOT*	McGown et al.[91]
	p-xylene	oleic acid	Koelmans et al.[92]
	p-xylene	stearic acid	"
	Toluene	Menhaden fish oil	Calvert et al.[93]
SiO_2	p-xylene	Na AOT	Damerell et al.[95]
TiO_2	p-xylene	Na AOT	McGown et al.[96]
$BaTiO_3$	MEK-ethanol	Emphos PS21-A†	Mikasa and Cannan [97]
	Toluene	Menhaden fish oil	Parrish et al.[94]
Carbon black	p-xylene	Na AOT	Damerell et al. [98]
$CaCO_3$	Benzene-Acetone	Na AOT	Damerell et al.[99]

*sodium dioctyl sulfosuccinate, American Cyanamid, Wayne, NJ

†phosphate ester, Witco Chemical Co., New York, NY

slips. One such alternative employs fired ceramic molds produced by a lost-wax process [15]. In this process, a wax form of the shape to be produced is made by injecting hot wax into a hard plastic negative of the shape. The resulting wax piece is then coated with the mold material, dried, and fired. The wax is eliminated in the firing process, leaving a mold of the desired shape.

Once the fired ceramic mold has been produced, a slip is poured into the mold. After the desired wall thickness has developed, the remainder of the slip is poured off and the ceramic casting is dried. After drying, the mold is peeled away from the cast ceramic, leaving a ceramic with a net shape identical to that of the original model. The stages of production of a ceramic nose cone from a metal preform are represented. The original metal form, a wax duplicate, a plastic negative of the metal form, a fired ceramic mold, and a cast ceramic are shown from left to right in Figure 7.

Optimization of the Slip Casting Process

The two critical factors that must be controlled in the production of cast ceramics are the viscosity of the slip and the particle size distribution. The amount of deflocculant required to produce a stable suspension of ceramic particulates is determined by monitoring the viscosity of the suspension with respect to the dispersant concentration. As dispersant is added to the slip, the viscosity decreases to a minimum value. At this concentration level the slip is said to be fully dispersed. Beyond this minimum, however, the

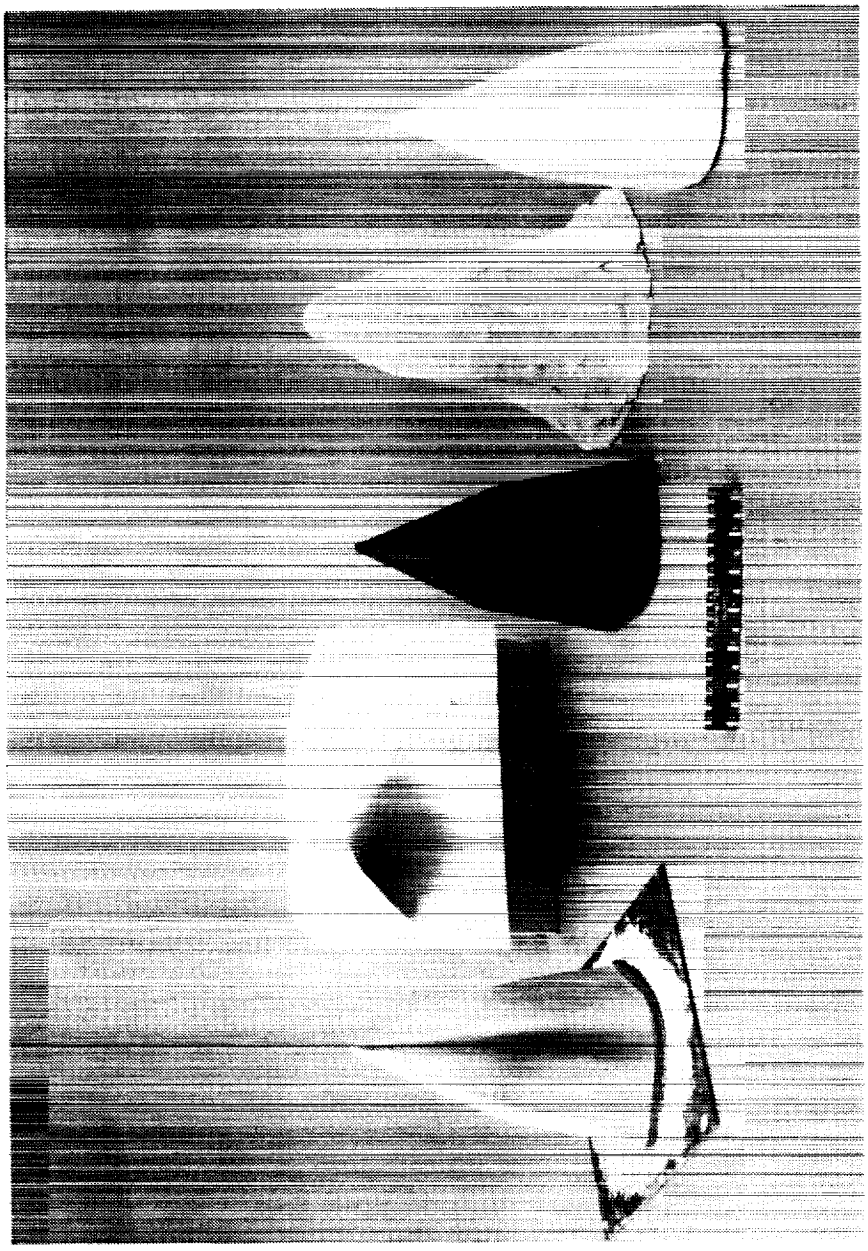

Figure 7. Stages of the lost wax process (Courtesy of P. Vasquez and G.M. Buck, NASA-Langley Research Center, Hampton, VA).

suspension will lose its stability due to the interaction of the excess dispersant and the dispersant occupying the particulate surfaces [70-71,89].

In addition to optimizing the dispersant concentration, the particle size distribution of the ceramic particulates must also be considered. Typically, slips contain ceramic powders ranging in size from 0.1 to 20 μm. The use of wide particle size distributions benefits both the rheological properties of the slip and the strength of the ceramic in both the dried and fired states [90]. These benefits are attributed to the increased packed density of the cast ceramic particles. Conversely, ceramics cast from narrow particle size distributions demonstrate relatively poor particle packing characteristics, resulting in poor handling strengths of the ceramics and larger fired shrinkages.

The effects of particle size distribution were first studied by Andreason [91]. He found that the optimum particle packing for a distribution was governed by the relation

$$\frac{CPFT}{100} = \left(\frac{D}{D_L}\right)^n , \qquad (1)$$

where CPFT represents the cumulative percent finer than, D is the size of particle in question, D_L is the size of the largest particle, and n is the distribution modulus. Andreason found that optimum packing occured when $0.33 < n < 0.50$.

Examination of the curves produced from Andreason's equation revealed a spread in the percentage undersize permissible at a given particle size. This aspect of Andreason's

equation was modified by Dinger and Funk [92] to include the smallest particle, D_s, in the distribution. The Dinger-Funk equation is

$$\frac{CPFT}{100} = \frac{D^n - D_s^n}{D_L^n - D_s^n} \quad . \tag{2}$$

According to this model, optimum particle packing is obtained when n is approximately 0.37.

Application of Slip Casting to Ceramic Superconductors

Slip casting ceramic superconductors offers two primary advantages over many of the shape forming processes used to produce superconducting devices. The first benefit is that slip casting techniques can reliably produce near net-shape ceramics [68-69]. The second benefit of slip casting is that the particles can be aligned in a magnetic field while the particles are in suspension. By magnetically texturing the superconductor during the casting process, the current transport properties of the superconductor may be significantly enhanced by overcoming the anisotropic nature of the material [47-55].

EXPERIMENTAL PROCEDURE

Synthesis of Y-Ba-Cu-O Powders

The $YBa_2Cu_3O_{7-x}$ compound used throughout this work was produced in 1 kg batches by the solid state reaction of Y_2O_3, $BaCO_3$, and CuO (see Appendix A) as described by Cava, et al [93]. In this process, stoichiometric amounts of the precursor powders were blended for 30 minutes in deionized water in a ball mill. The powder was subsequently poured into a stainless steel pan, dried at 90 °C for 18 hours, pressed into 2.5 cm diameter compacts at 37 MPa, and calcined for 8 hours at 900°C. Upon cooling, the compacts were crushed with a mortar and pestal, pressed, and calcined as before. This procedure was repeated a total of three times. A schematic representation describing the production of the superconducting compound is shown in Figure 8.

Production of the $YBa_2Cu_3O_{7-x}$ phase was verified by pressing 15g of powder in a 1 inch diameter stainless steel die at 1.85 GPa and firing the resulting disk to 940°C for 6 hours. The test specimen was then annealed in flowing oxygen at 650°C for 16 hours. Silver-doped (10%) $YBa_2Cu_3O_{7-x}$ specimens were prepared by blending the appropriate amount of Ag_2O with superconductive powder, pressing the blend into a compact, and firing as before. The fired ceramics were characterized by a standard d.c. four probe measurement (see Appendix B), Cu Kα X-ray diffraction, and scanning electron microscopy (SEM).

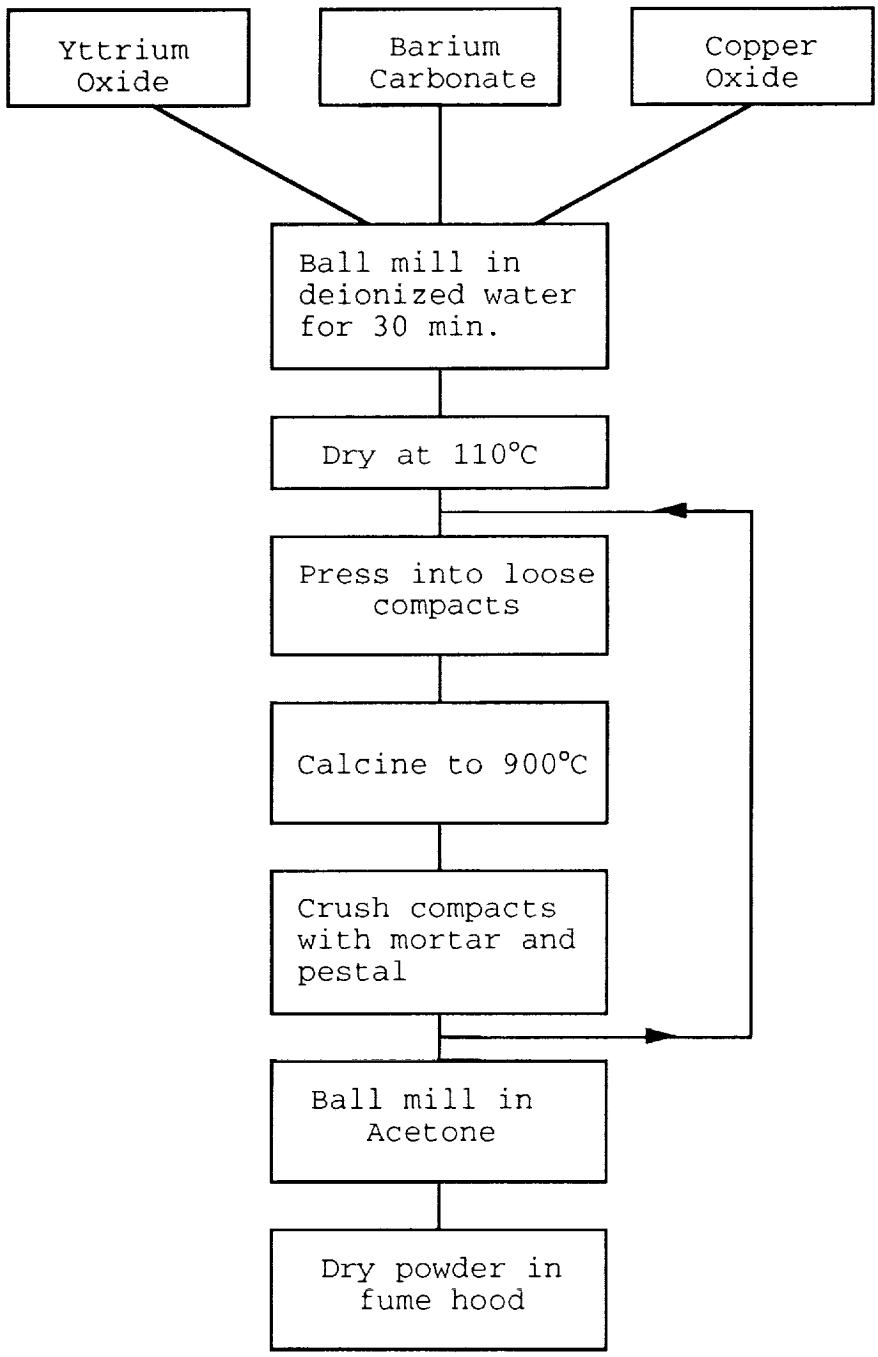

Figure 8. Flow diagram describing the production of $YBa_2Cu_3O_{7-x}$ powder.

Once the $YBa_2Cu_3O_{7-x}$ compound was prepared, the material was ball milled to obtain powders for experimentation. The synthesized material was ball milled in acetone in porcelain milling jars using alumina grinding media. The particle size distribution of the milled powder was obtained using a Shimadzu Laser Diffraction Particle Size Analyzer (Model SALD 1100). Additionally, the density of the powder was obtained by a standard Archimedian method as described by Lowell and Shields [94].

Evaluation of Solvent/Dispersant Systems

The first phase in the development of the non-aqueous slip casting process was the determination of a suitable solvent-dispersant system to use as the carrier liquid for the superconductive powders. The objective of this investigation was to identify a solvent/dispersant system that imparts stability to the suspension over a wide range of dispersant concentrations.

Six solvent/dispersant systems were selected for testing. The dispersants selected included three branched hydrocarbons (Menhaden fish oil, oleic acid, and stearic acid), two phosphates (Emphos PS21A and Merpol A), and one sodium-containing dispersant (Aerosol OT). The trade name, chemical composition, and molecular weight of each of the six dispersants tested are shown in Table 6.

To evaluate the solvent/dispersant systems, the viscosity of each suspension was measured as a function of the volume percent of dispersant added. A Brookfield Digital Viscometer

Table 6. Commercial names, chemical compositions, and molecular weights of dispersants tested.

Dispersant	Chemical Formula	Molecular Weight
Oleic Acid*	$CH_3(CH_2)_7CH=CH(CH_2)_7COOH$	282
Stearic Acid*	$CH_3(CH_2)_{16}COOH$	284
Menhaden Fish Oil**	$[CH_3(CH_2)_7CH=CH(CH_2)_7COOCH]_3$	881
Emphos PS21A†	$HO(PO_2)_xO(CH_2)_yCH_3$	530/950
Merpol A††	Proprietary	---
Aerosol OT†††	$CH_3(CH_2)_7O(CO)CH_2CH(SO_3^-Na^+)(CO)OCH_3(CH_2)_7$	444

*Fisher Scientific, Raleigh, NC

**Reichhold Chemical, Newark, NJ

†50% mono-;50% dialkyl phosphate esters, Witco Chemical Company, New York, NY

††ethoxylated phosphate, E.I. DuPont de Nemours & Co., Wilmington DE

†††sodium dioctyl sulfosuccinate, American Cyanamid, Wayne, NJ

Model DV-II with a number 63 spindle was used to obtain the viscosity of the slurries. A standard shear rate of 20 sec^{-1} was used in each of these experiments.

For each suspension evaluated, a standard solids loading of 35 volume percent (approximately 80 percent by weight) was employed. The $YBa_2Cu_3O_{7-x}$ powder used possessed a mean particle size of approximately 5μm and a density of 5.5 g/cm^3. The particle size distribution for the powder used in these studies is given in Figure 9, and the six solvent/dispersant combinations tested are shown in Table 7.

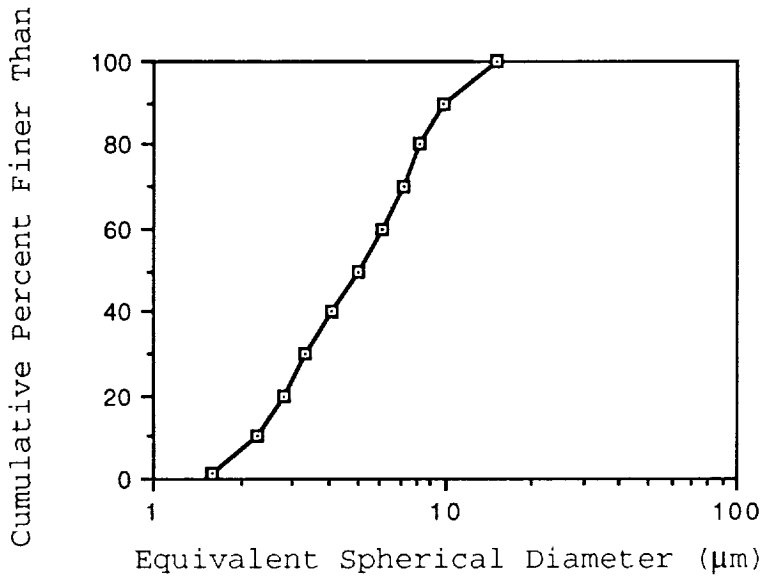

Figure 9. Particle size distribution of $YBa_2Cu_3O_{7-x}$ powder used in rheological experiments.

Table 7. Solvent/dispersant combinations evaluated.

Dispersant	Solvent
Menhaden Fish Oil	Acetone
Oleic acid	Xylene
Stearic acid	Xylene
Emphos PS21A	Methyl ethyl ketone
Merpol® A	Acetone
Aerosol OT	Xylene

Demonstration of Nonaqueous Casting Process

To demonstrate the compatibility of organic slips and fired ceramic molds to produce uniquely shaped $YBa_2Cu_3O_{7-x}$ ceramics, several castings were made using acetone as the carrier liquid and Menhaden fish oil as the dispersant. In this initial investigation, simple rectangular specimens were produced.

The slips used in this phase of the research were composed of powders with the same characteristics as those employed in the evaluation of solvent/dispersant systems. The $YBa_2Cu_3O_{7-x}$ powder was dispersed in acetone using 1.25 volume percent Menhaden fish oil as the dispersant.

The molds used in this work were prepared by a lost wax process as described by Vasquez and Buck [15]. In this procedure, wax preforms of the desired shape were coated with a calcium sulfate bonded blend of silica, fiberglass, and refractory materials (R & R 909 Investment, Ransom and Randolph, Maumee, OH) and dried at room temperature. The coated wax pieces were then fired to 540°C using a heat up rate of 3°C/min and held at the peak temperature for 2 hours. During the firing process, the wax preform was lost, leaving a fired ceramic mold in the

same shape as the wax preform. The resulting molds possessed wall thicknesses of approximately 0.5 cm.

To cast the $YBa_2Cu_3O_{7-x}$ ceramics, the nonaqueous slips were poured into the molds as in traditional casting operations. Once formed, the castings were dried at room temperature for several hours and then placed in a dryer at 45°C for two additional hours to eliminate any remaining solvent. Next, the castings were removed from the mold by peeling the mold away from the superconductor. After demolding, the cast ceramics were fired at 940°C for 6 hours, followed by an oxygen annealing treatment at 500°C for 15 hours. Superconductivity in the cast ceramics was verified by both a Meissner effect and d.c. four-probe resistance measurements (see Appendix B). Additionally, the microstructures were evaluated using a scanning electron microscope.

To determine the uniformity of the cast ceramics, five cross-sectional specimens were cut at various lengths along a 1 x 2.5 x 4.0 cm ceramic, and the critical current density (see Appendix C) of each section was measured at 77 K.

Evaluation of Critical Process Variables

To determine the critical process parameters of the nonaqueous slip casting process, four variables were selected and a full four-factor factorial experiment [95] was carried out. The four variables chosen for evaluation were (1) the sintering temperature, (2) the particle size distribution of the $YBa_2Cu_3O_{7-x}$ powder, (3) the solids loading of the slip, and

(4) the silver dopant level. Values for the high and low experimental levels are given in Table 8, and a schematic of the experimental design is shown in Figure 10. The upper and lower case letters seen in Table 8 and Figure 10 represent the high and low levels chosen for the respective variables.

In this work, the particle size distributions were characterized by a distribution modulus, n, as described by Dinger and Funk [92]. The two particle size distributions chosen as high and low experimental levels are shown in Figure 11. The particle size distriutions were obtained by ball milling 1 kg of $YBa_2Cu_3O_{7-x}$ powder in a 1 liter porcelain milling jar with 500 ml of acetone and 900 g of Al_2O_3 grinding media (1.27 cm high, 1.27 cm diameter). The two particle size distributions shown in Figure 11 were obtained by milling for 16 (n = 0.65) and 24 hours (n = 0.40). The $YBa_2Cu_3O_{7-x}$ and $Ag_2O/YBa_2Cu_3O_{7-x}$ powder blends used in these experiments possessed densities of 5.5 and 6.0 g/cm^3 respectively.

For each of the sixteen (16) experimental conditions, three 1 x 2.5 x 4.0 cm rectangular specimens were cast. After removal of the mold, each specimen was fired according to the experimental design with an 8 hour soak time at the peak temperature, and then annealed in flowing oxygen at 650°C for 16 hours. The fired shrinkage, relative density, and critical current density of the fired ceramics were used as criteria for the statistical comparison of the cast ceramics.

Table 8. High and low levels for experimental variables.

Variable	Low level	High level
Sintering temperature	935°C (a)	945°C (A)
Particle size	n = 0.40 (b)	n = 0.65 (B)
Solids loading	70 wt. percent (c)	80 wt. percent (C)
Ag dopant level	None (d)	10% (D)

		945°C		935°C	
		n=0.65	n=0.40	n=0.65	n=0.40
80 wt%	10% Ag				
	No Ag				
70 wt%	10% Ag				
	No Ag				

Figure 10. Schematic of the four factor factorial design [95].

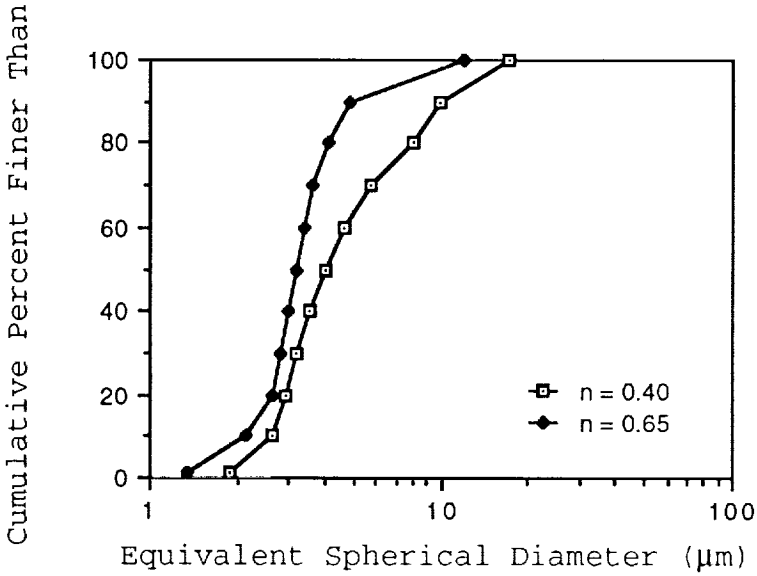

Figure 11. Particle size distributions of $YBa_2Cu_3O_{7-x}$ powders used in factorial experiment.

The volume fired shrinkage (%VFS) was calculated using the relation [96]

$$\%VFS = \frac{V_d - V_F}{V_d} \times 100\% \qquad (3)$$

where V_d and V_F are the values of the ceramic in the dried and fired states respectively. These calculations were based on dimensional measurements made prior to firing and after oxygen annealing.

The bulk density (ρ_B) of the specimens was obtained by employing a standard Archemedian technique [96]. In this procedure, the dry weight (W_{Dry}), suspended weight (W_{Sus}), and saturated weight (W_{Sat}) of the ceramics were measured using a balance with a basket suspended beneath in a xylene bath. In this case, the density of the liquid, ρ_L, was 0.8611 g/cm^3 [79]. The bulk density was calculated using the following relation:

$$\rho_B = \frac{W_{Dry}\rho_L}{W_{Sat} - W_{Sus}} \quad . \qquad (4)$$

Once the bulk density was determined, the percentage of theoretical density (or relative density, ρ_B/ρ_{TH}) was calculated. The relative density was determined assuming the theoretical density of the $YBa_2Cu_3O_{7-x}$ compound to be 6.38 g/cc, and the theoretical density of 10% Ag-doped $YBa_2Cu_3O_{7-x}$ to be 6.79 g/cc [97].

The specimens for critical current density measurement were prepared by cutting a cross-sectional segment from each

cast bar. The current density of each specimen was measured at 77 K as described in Appendix C.

Once all of the experimental data was obtained, analysis of variance (ANOVA) calculations were performed on the three data sets (i.e., fired shrinkage, relative density and J_c). A review of the ANOVA calculations is provided in Appendix D.

Application of Magnetic Alignment

To determine the feasibility of using magnetic fields to orient the $YBa_2Cu_3O_{7-x}$ grains during the casting process, several castings were performed with molds mounted in a 0.7 Tesla (T) magnetic field as shown in Figure 12. In this procedure, cylindrical and rectangular specimens approximately 2 cm in length with cross-sectional areas on the order of 0.5 cm^2 were cast. These ceramics were cast and fired using the optimum process conditions as determined in the previous section.

Once produced, SEM analyses were performed on several of the specimens to examine the alignment of the grains. X-ray diffraction was also employed to determine the degree of preferential orientation induced by the presence of the magnetic field during the casting process. Additionally, the critical current density of these cast specimens was measured along the direction cast perpendicular to the applied magnetic field (i.e., along the ab-plane).

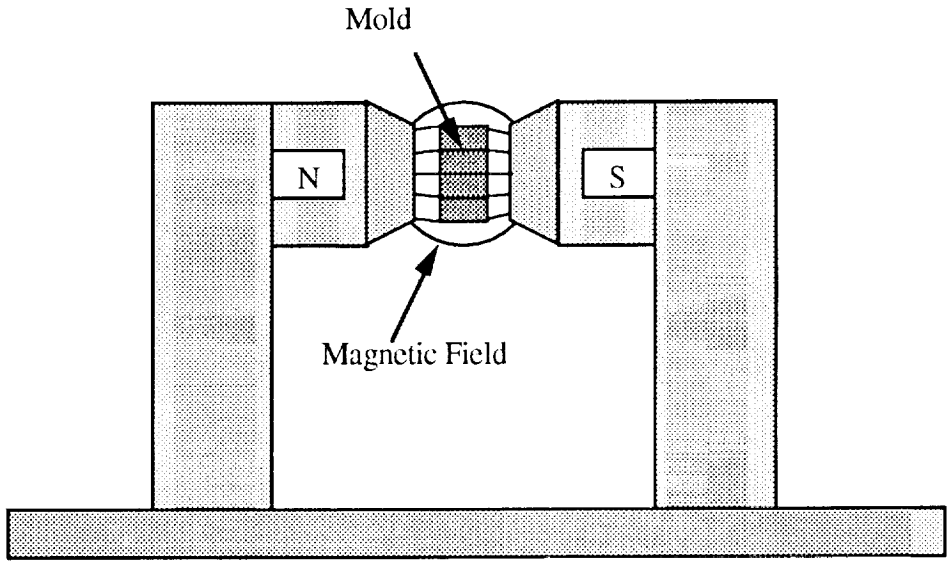

Figure 12. Experimental arrangement for slip casting in a magnetic field.

RESULTS AND DISCUSSION

Synthesis of Y-Ba-Cu-O Powders

Electrical resistance vs. temperature measurements and X-ray diffraction confirmed that the solid state synthesis technique produced phase-pure superconductive $YBa_2Cu_3O_{7-x}$. The $YBa_2Cu_3O_{7-x}$ and Ag-doped $YBa_2Cu_3O_{7-x}$ compounds possessed sharp superconductive transitions near 90 K. Additionally, the results of the X-ray diffraction analyses were in agreement with reported data [30,93]. Resistance versus temperature data and X-ray diffraction results are shown in Figures 13 and 14 for $YBa_2Cu_3O_{7-x}$ and Figures 15 and 16 for Ag doped $YBa_2Cu_3O_{7-x}$.

The SEM analyses of the microstructures showed that the $YBa_2Cu_3O_{7-x}$ specimens possessed randomly oriented, rectangular grains, which are typically observed for these materials [98-99]. An example of the fired microstructure of a $YBa_2Cu_3O_{7-x}$ is shown in Figure 17. The silver-doped specimens possessed similar grain structures; however, less open porosity was observed due to the filling of the pores by the silver [27-31]. The migration of the silver to the open pores in the fired ceramic is shown in Figure 18. The black regions observed in the micrograph are pockets of silver within the polycrystalline ceramic.

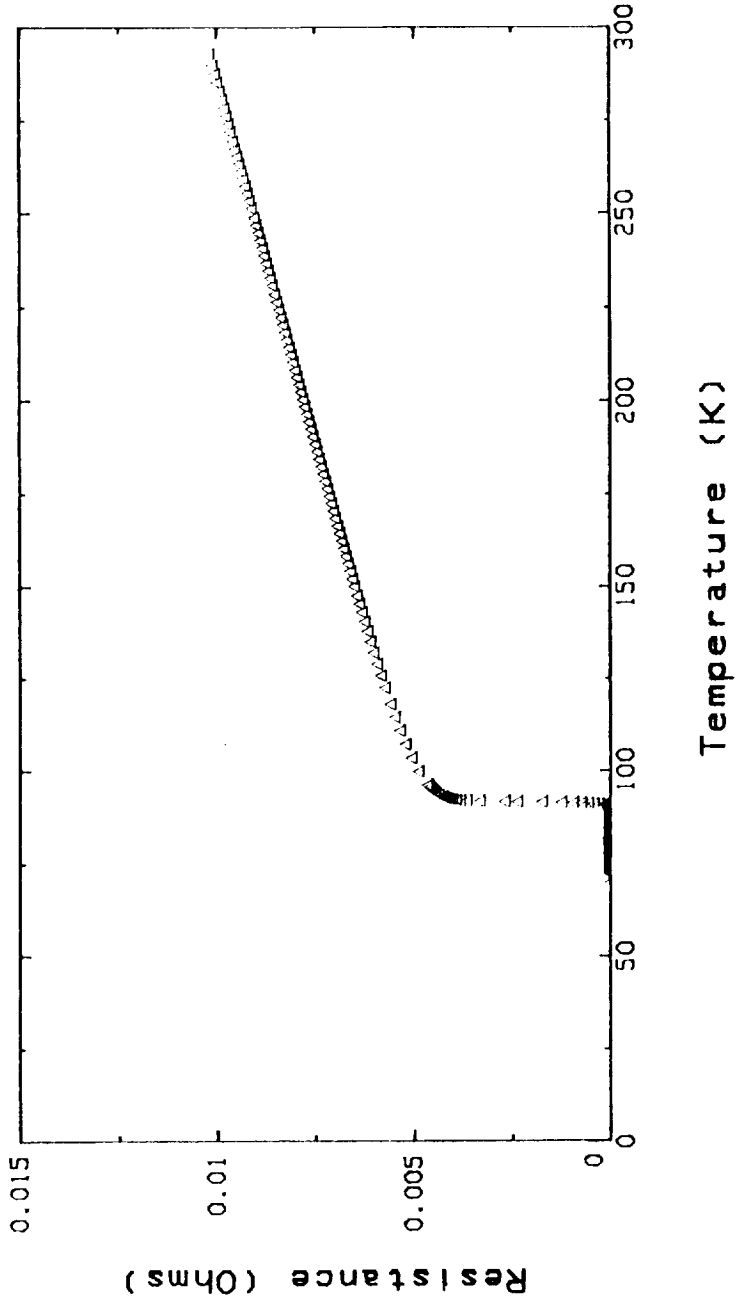

Figure 13. Resistance versus temperature data for $YBa_2Cu_3O_{7-x}$.

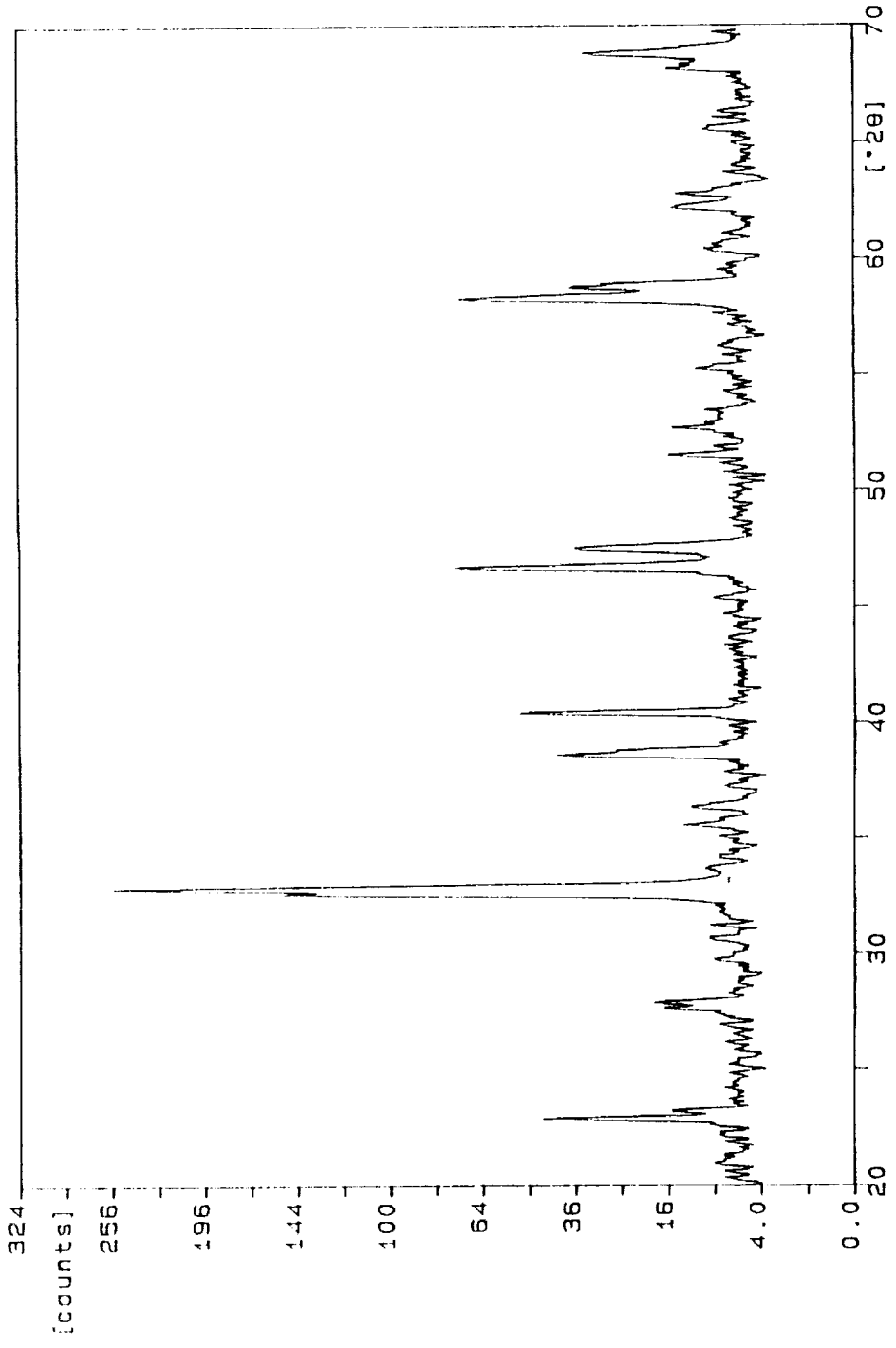

Figure 14. X-ray diffraction pattern for $YBa_2Cu_3O_{7-x}$.

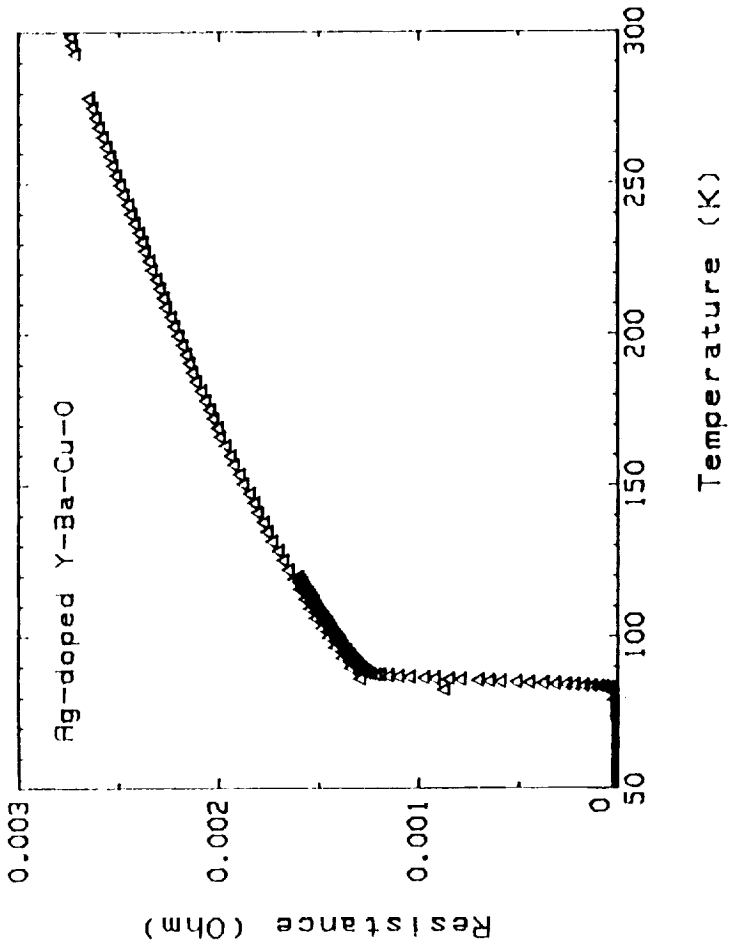

Figure 15. Resistance versus temperature data for 10% Ag-doped $YBa_2Cu_3O_{7-x}$.

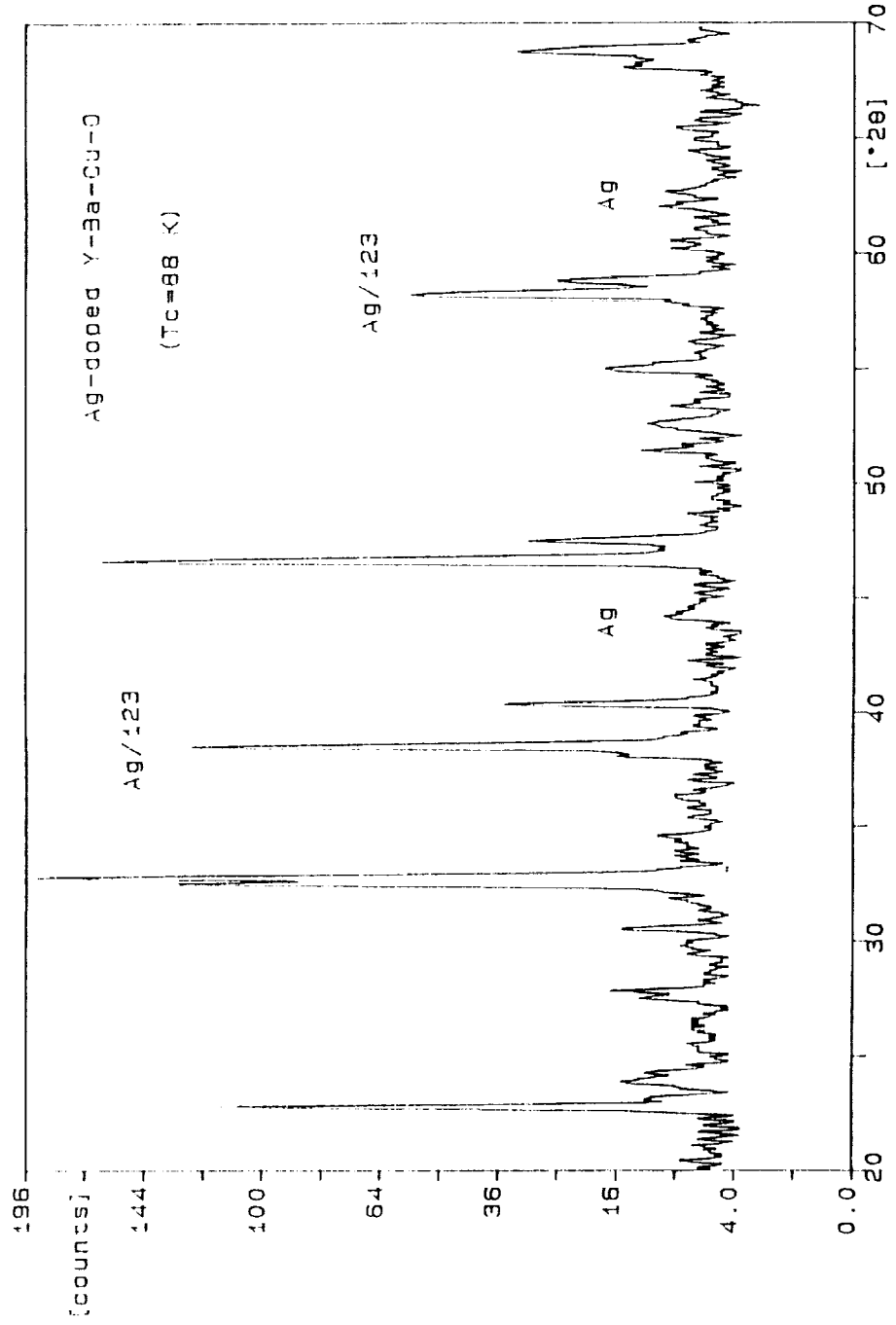

Figure 16. X-ray diffraction pattern for 10% Ag-doped $YBa_2Cu_3O_{7-x}$.

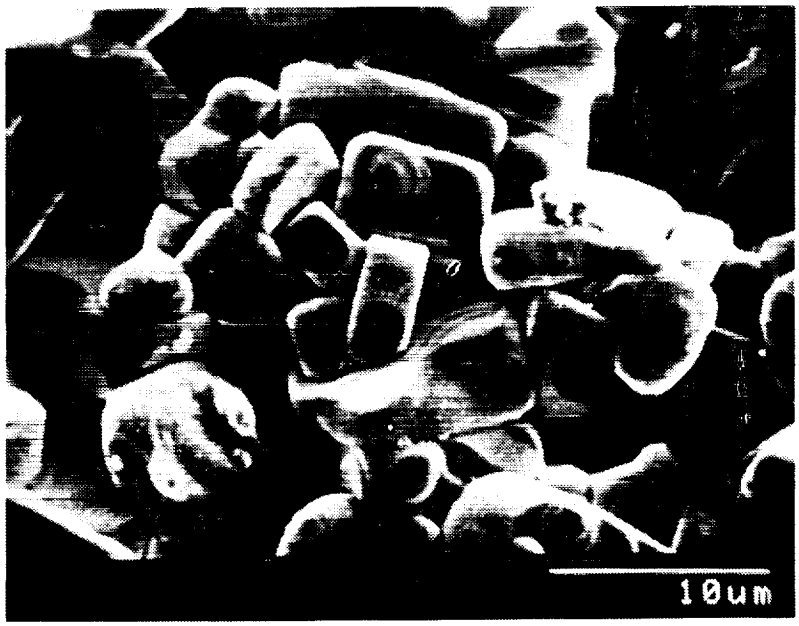

Figure 17. SEM micrograph showing rectangular grains in a $YBa_2Cu_3O_{7-x}$ specimen.

Figure 18. SEM micrograph of 10% Ag-doped $YBa_2Cu_3O_{7-x}$, where the dark regions are pockets of silver.

Evaluation of Solvent/Dispersant Systems

Of the three nonionic dispersant combinations tested, the Menhaden fish oil/acetone and the oleic acid/xylene systems possessed viscosity minima between 80 and 85 cps as shown in Figures 19 and 20. The viscosity minimum for the Menhaden fish oil in acetone system remained relatively constant over dispersant levels ranging from 0.75 to 1.75 volume percent. However, the viscosity minimum for the oleic acid/xylene system was constant over only a narrow range of dispersant concentrations (0.25 to 0.5 volume percent).

The stearic acid/xylene system, behaved differently, exhibiting an increase in viscosity as the dispersant level was increased, as shown in Figure 21. In this system, the lowest viscosity observed was 310 cps at the minimum dispersant concentration level of 0.25 volume percent.

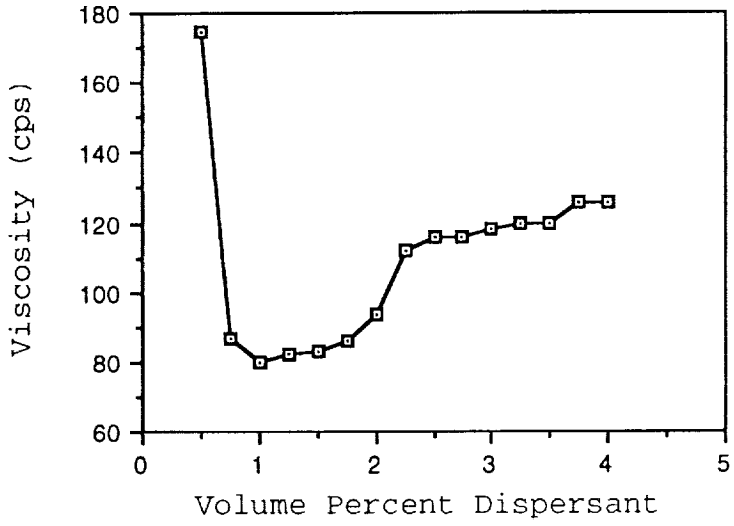

Figure 19. Viscosity versus dispersant concentration curve for $YBa_2Cu_3O_{7-x}$ powder dispersed in acetone with Menhaden fish oil (shear rate = $20.sec^{-1}$).

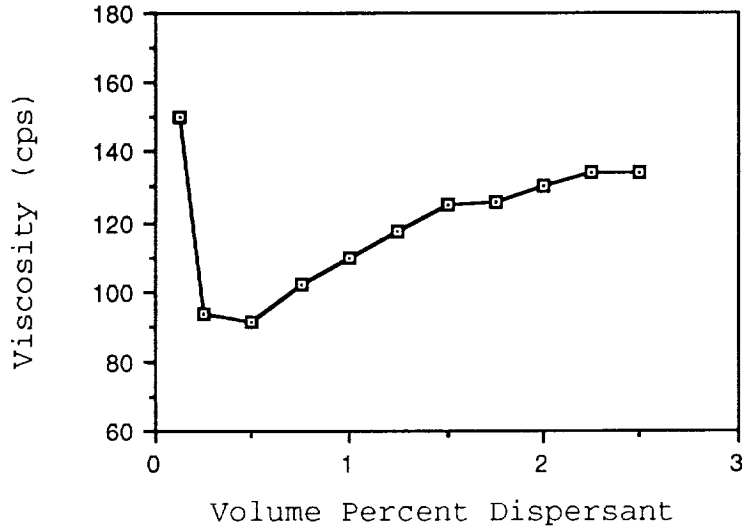

Figure 20. Viscosity versus dispersant concentration curve for $YBa_2Cu_3O_{7-x}$ powder dispersed in xylene with oleic acid (shear rate = $20.sec^{-1}$).

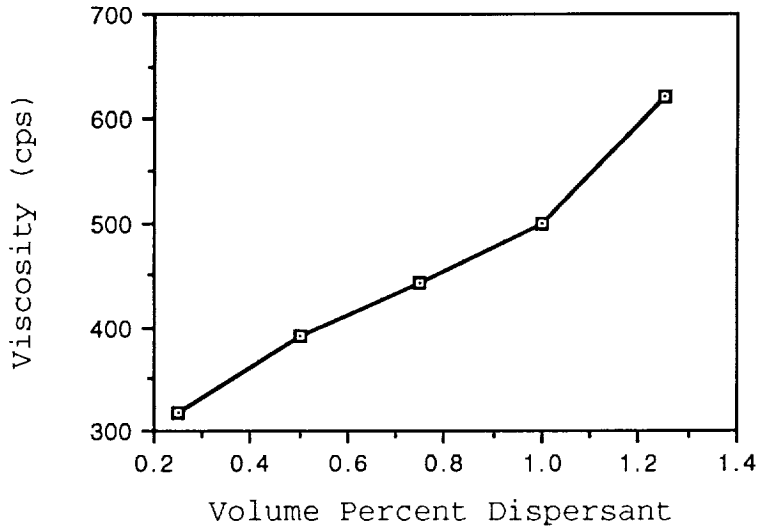

Figure 21. Viscosity versus dispersant concentration curve for $YBa_2Cu_3O_{7-x}$ powder dispersed in xylene with stearic acid (shear rate = $20.sec^{-1}$).

The two phosphate-containing dispersant systems evaluated (Emphos PS21A in MEK and Merpol® A in acetone) exhibited significantly different rheological behaviors than the nonionic dispersants. Both slips possessed narrow regions of full deflocculation at dispersant concentrations between 0.25 and 0.5 volume percent. In this concentration range, the slurries possessed viscosities on the order of 25-35 cps as shown in Figures 22 and 23. However, beyond this stable region, the $YBa_2Cu_3O_{7-x}$ powders began to settle out of suspension, indicating that complete deflocculation of the ceramic powders was possible only over narrow dispersant concentration ranges. Both the low viscosity values and narrow stability regions in these systems have been reported by Cannon [86].

The cationic dispersant system (Na AOT in xylene) also possessed a narrow region of stability at a dispersant concentration between 1 and 1.5 volume percent, as shown in Figure 24. Above and below this concentration range, the powders settled out of suspension.

The rheological behavior of each of the $YBa_2Cu_3O_{7-x}$ suspensions may be explained in terms of both the chemical composition and molecular architecture of the dispersant tested. The similarity in behavior between fish oil and oleic acid can be attributed to the similar molecular architectures of these two compounds. Both possess lyophobic carboxyl (-COOH) groups which attach to the particulate surfaces with hydrocarbon chains that are soluble in the surrounding liquid phase. Furthermore, these hydrocarbon chains are kinked at the carbon-

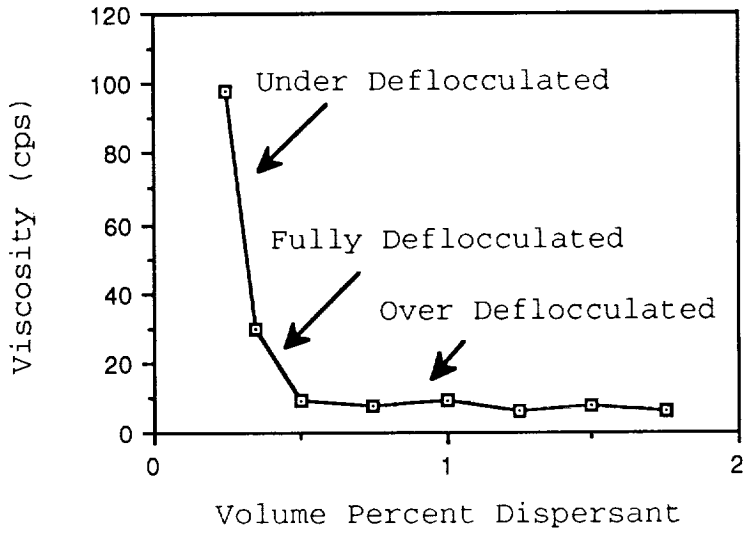

Figure 22. Viscosity versus dispersant concentration curve for $YBa_2Cu_3O_{7-x}$ powder dispersed in MEK with Emphos PS21A (shear rate = $20.sec^{-1}$).

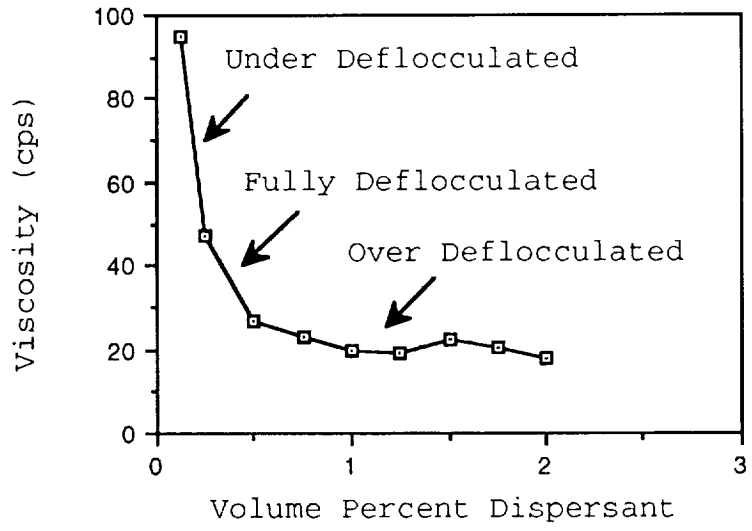

Figure 23. Viscosity versus dispersant concentration curve for $YBa_2Cu_3O_{7-x}$ powder dispersed in acetone with Merpol® A (shear rate = $20.sec^{-1}$).

carbon double bond shown in Figure 25 as described by Doroszkowski and Lambourne [100]. They found that this kinked structure provided better resistance to flocculation in sterically stabilized systems by reducing the distance from the particulate surface at which the polymeric chains may interact.

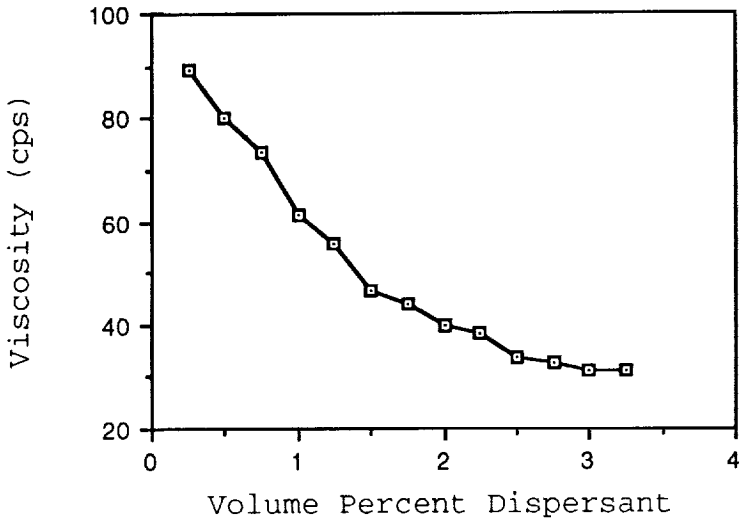

Figure 24. Viscosity versus dispersant concentration curve for $YBa_2Cu_3O_{7-x}$ powder dispersed in xylene with Na-AOT (shear rate = $20.sec^{-1}$).

In the case of the stearic acid system, no minimum viscosity was observed although no settling of the ceramic powders was noted. These relatively high viscosity values may be attributed to the long, straight polymeric nature of the stearic acid structure as seen in Figure 25 (c). These long chains interact with one another farther away from the particulate surface than branched hydrocarbons, increasing the viscosity of the suspension [74-78, 85].

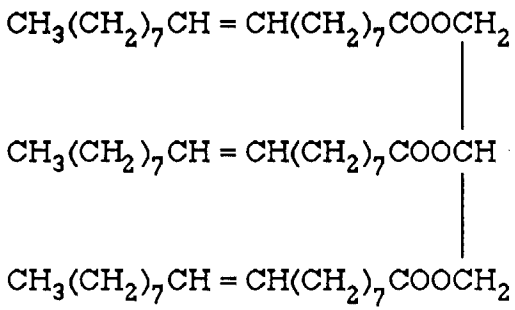

(a) Menhaden fish oil

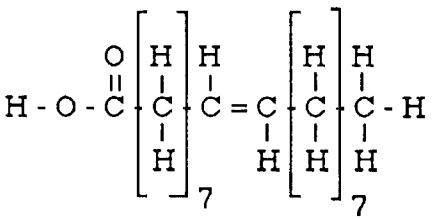

(b) oleic acid

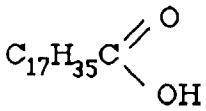

(c) stearic acid

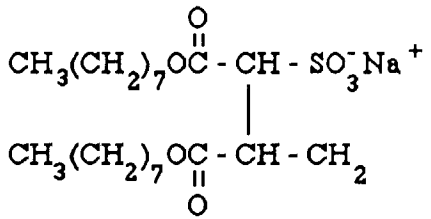

(d) sodium dioctly sulfosuccinate (Aerosol OT)

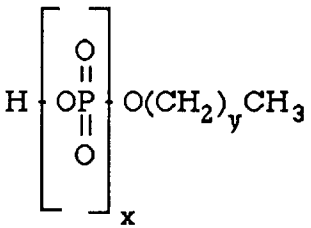

(e) phosphate ester (Emphos PS21A)

Figure 25. Molecular architectures of (a) Menhaden fish oil, (b) oleic acid, (c) stearic acid, (d) sodium dioctyl sulfosuccinate, and (e) phosphate ester dispersants.

Like the nonionic systems, the rheological properties of the phosphate and Aerosol® systems tested may also be explained in terms of the molecular compositions and architectures of these dispersants. As observed in Figures 23 through 25, each of the slips possessed a decrease in viscosity until full deflocculation was obtained. Beyond this point, however, the behaviors differed. In these systems, the presence of excess electrolytes resulted in the flocculation of the ceramic powders, and the subsequent settling of the powders out of suspension.

Of the various organic dispersants available for use in nonaqueous systems, Menhaden fish oil is generally considered to be the most effective dispersant because it possesses more carboxyl groups along with a greater number of nonlinear chains. These additional lyophobic and lyophilic components promote the stability of these systems in comparison to other dispersants [82-83]. The results of the rheological studies support these findings, as the slurries utilizing Menhaden fish oil as a dispersant possessed a stable viscosity over the widest concentration range as compared to the other dispersants tested.

Demonstration of Nonaqueous Slip Casting Process

The nonaqueous slip casting of $YBa_2Cu_3O_{7-x}$ slips into foundry molds was similar to more traditional slip casting operations in that the cast ceramic took the shape of the mold due to the removal of the carrier liquid from the interior of the

mold by capillary action. The feasibility of employing this process to produce simple net-shape superconductors is shown in Figure 26. In this photograph, a rectangular wax preform, a fired ceramic mold (or foundry mold), and a fired superconductor are shown from left to right.

After the cast ceramics were fired and oxygen treated, they were found to exhibit a Meissner effect similar to that of pressed compacts. Furthermore, these cast superconductors possess sharp superconducting transitions at approximately 90 K as shown in Figure 27.

The SEM evaluation of the fired microstructures showed that these cast superconductors possess the randomly oriented, rectangular grain structures similar to those of the superconductive test specimens previously observed (see Figure 17). An SEM micrograph of the grain structure of a slip cast specimen is shown in Figure 28.

The uniformity of these cast superconductors was verified by analyzing the critical current density of five cross-sectional specimens cut from a single rectangular specimen. Each section possessed a critical current density of approximately 25 A/cm^2 ($\pm$ 1.7%), indicating that the electrical properties of the ceramics were uniform throughout the cast body.

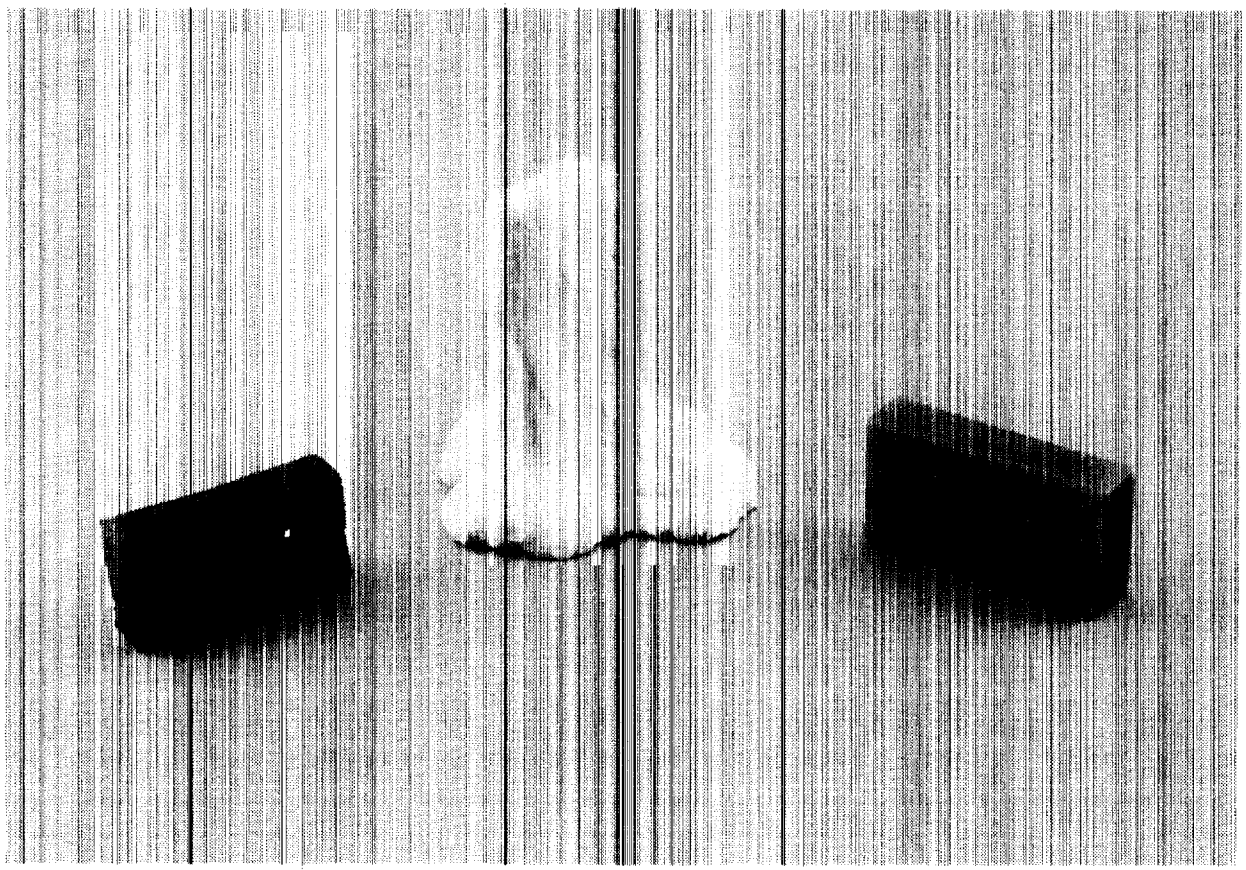

Figure 26. Stages of the nonaqueous slip casting process including a wax preform (left), a fired ceramic mold (center), and a fired superconductor (right).

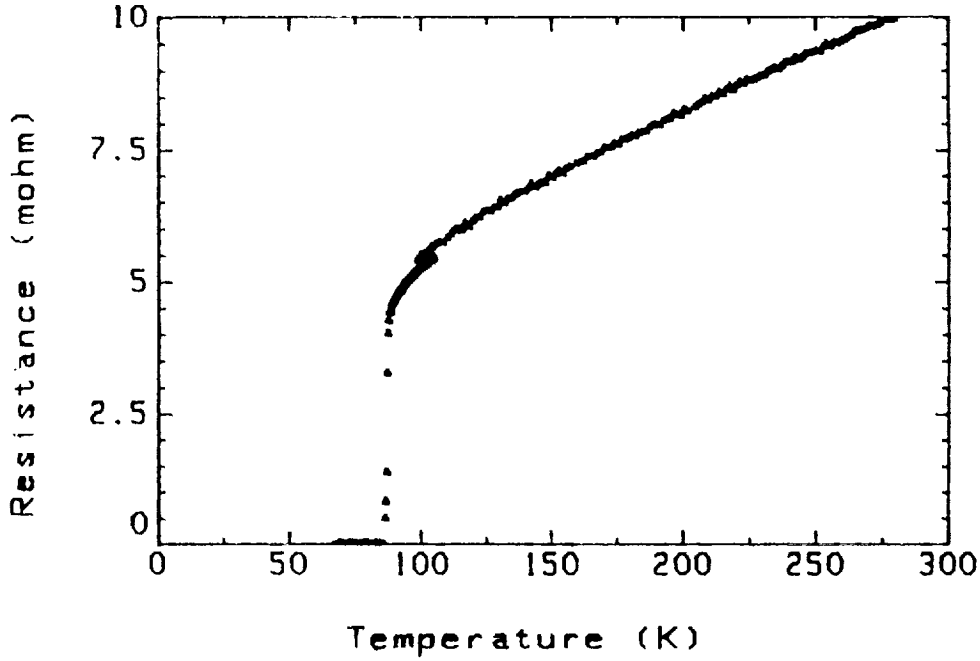

Figure 27. Resistance versus temperature curve for slip cast $YBa_2Cu_3O_{7-x}$.

Figure 28. SEM micrograph of the grain structure of slip cast $YBa_2Cu_3O_{7-x}$.

Evaluation of Critical Process Parameters and ANOVA

The analysis of variance (ANOVA) results, shown in Table 9, indicate that the sintering temperature (A) and the particle size distribution (B) employed significantly influenced the fired shrinkage, relative density, and critical current density at a 1% level. The interaction between these two process variables (AB) also significantly affected these properties at a 1% level. The significance of these variables is evidenced by the experimental data shown in Tables 10-12. Furthermore, these results indicate that these two process variables and their interaction can be controlled to optimize the properties of the superconductive ceramics.

The use of silver dopants (D) was also found to significantly impact the relative density and Jc of the cast ceramics. However, in all cases, the addition of silver resulted in the production of specimens with relatively poor properties (i.e., high shrinkages and low densities and critical current densities). Several primary (AD, BD, CD) and one secondary (ABD) interaction involving silver dopants were also found to be significant at a 1% level. The significance of these interactions may be attributed to the variability in the data for silver doped specimens as shown in Tables 10-12.

The difference between experimental levels for the solids loading within the slip (C) was not found to be significant. The resistance of the casting process to small fluctuations in the solids loading is important, as minor variations due to

Table 9. Calculated F values from the ANOVA calculations.

Source	F (Shrinkage)	F (ρ_{rel})	F (J_c)
A	44175.15*	17.00*	1876929.65*
B	6723.74*	38.10*	1175886.73*
C	5.19	0.87	5.61
D	193651.05*	23.10*	1781075.21*
AB	231854.53*	22.66*	1188765.46*
AC	7.47	4.11	7.98*
AD	5115.23*	0.64	1796917.20*
BC	0.21	2.92	4.78
BD	50643.01*	5.50	1265665.20*
CD	0.21	7.10	4.78
ABC	0.83	0.01	6.98
ABD	8892.14*	4.68	1252375.32*
ACD	0.00	0.09	3.00
BCD	5.19	1.57	5.61
ABCD	0.00	0.00	3.66

*Indicates significance at a 1% level.

Table 10. Fired shrinkage data (percent volume shrinkage) obtained in factorial experiment.

		A (945°C)		a (935 °C)	
		B(n=0.65)	b(n=0.40)	B(n=0.65)	b(n=0.40)
C (80 Wt. %)	D(10% Ag)	38.2 37.8 37.3	47.6 46.9 48.1	33.2 34.9 34.0	30.1 29.5 29.2
	d(No Ag)	33.9 33.7 32.8	37.7 38.8 38.6	30.6 30.2 30.9	14.4 14.6 14.1
c (70 Wt %)	D(10% Ag)	36.5 39.2 38.1	47.4 48.1 47.2	34.4 34.2 33.6	28.7 30.4 29.6
	d(No Ag)	33.8 32.7 34.1	37.9 38.4 39.1	30.2 29.8 31.5	13.8 14.4 15.0

Table 11. Relative density data obtained in factorial experiment.

		A (945°C)		a (935 °C)	
		B(n=0.65)	b(n=0.40)	B(n=0.65)	b(n=0.40)
C (80 Wt. %)	D(10% Ag)	0.84 0.74 0.93	0.52 0.56 0.65	0.92 0.91 0.84	0.66 0.74 0.79
	d(No Ag)	0.85 0.83 0.84	0.68 0.64 0.58	0.83 0.83 0.84	0.91 0.85 0.89
c (70 Wt %)	D(10% Ag)	0.81 0.75 0.71	0.71 0.65 0.47	0.71 0.71 0.77	0.54 0.70 0.78
	d(No Ag)	0.90 0.91 0.87	0.73 0.65 0.74	0.82 0.83 0.83	0.87 0.88 0.92

Table 12. Critical current density (A/cm^2) data obtained in factorial experiment.

		A (945°C)		a (935 °C)	
		B(n=0.65)	b(n=0.40)	B(n=0.65)	b(n=0.40)
C (80 Wt. %)	D(10% Ag)	0.1 0.4 0.6	0.0 0.0 0.0	1.3 1.5 1.1	0.02 0.02 0.02
	d(No Ag)	0.0 0.0 0.0	0.0 0.0 0.0	8 10 10	85 75 110
c (70 Wt %)	D(10% Ag	0.3 0.1 0.7	0.0 0.0 0.0	0.8 1.3 1.7	0.00 0.03 0.05
	d(No Ag)	0.0 0.0 0.0	0.0 0.0 0.0	10 8 9	115 90 75

solvent evaporation could occur in the production of larger specimens.

As shown in Table 10, fired shrinkages ranging from 33 to 48 volume percent were observed in experiments where $YBa_2Cu_3O_{7-x}$ specimens were fired at 945°C and in all of the specimens containing silver dopants. Each of the $YBa_2Cu_3O_{7-x}$ specimens prepared under these conditions possessed visible green regions on the surface, indicating that the $YBa_2Cu_3O_{7-x}$ phase had undergone a peritectic decomposition to form Y_2BaCuO_5 and a $BaCuO_2$ liquid as described by Jin et al [101]. A phase diagram illustrating this melting behavior is shown in Figure 29.

The high shrinkage values obtained for specimens fired at 945°C are attributable to the presence of a reactive liquid phase [102], in this case $BaCuO_2$. An X-ray diffraction pattern showing the presence of the Y_2BaCuO_5 and $BaCuO_2$ decomposition phases in a slip cast $YBa_2Cu_3O_{7-x}$ specimen fired at 945°C is shown in Figure 30. Additionally, an SEM micrograph showing the small, needle-like grains indicative of the Y_2BaCuO_5 decomposition phase [103] is shown in Figure 31.

The addition of silver to $YBa_2Cu_3O_{7-x}$ ceramics further decreased the onset temperature of liquid phase sintering.[43-46] The increased quantity of a reactive liquid resulted in the high shrinkage values obtained for all of the silver-doped specimens.

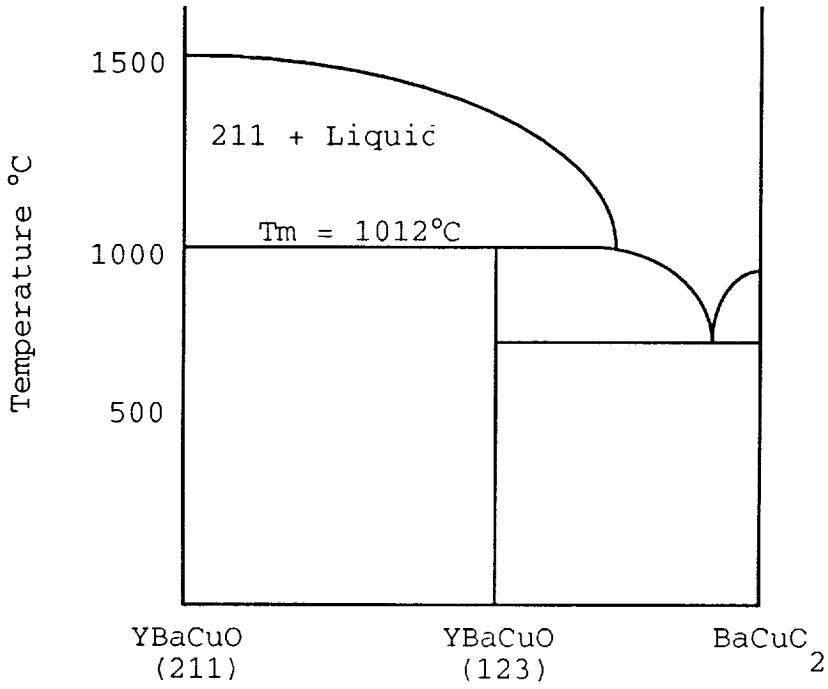

Figure 29. Y_2BaCuO_5-$BaCuO_2$ binary phase diagram (After Jin et al.[101]).

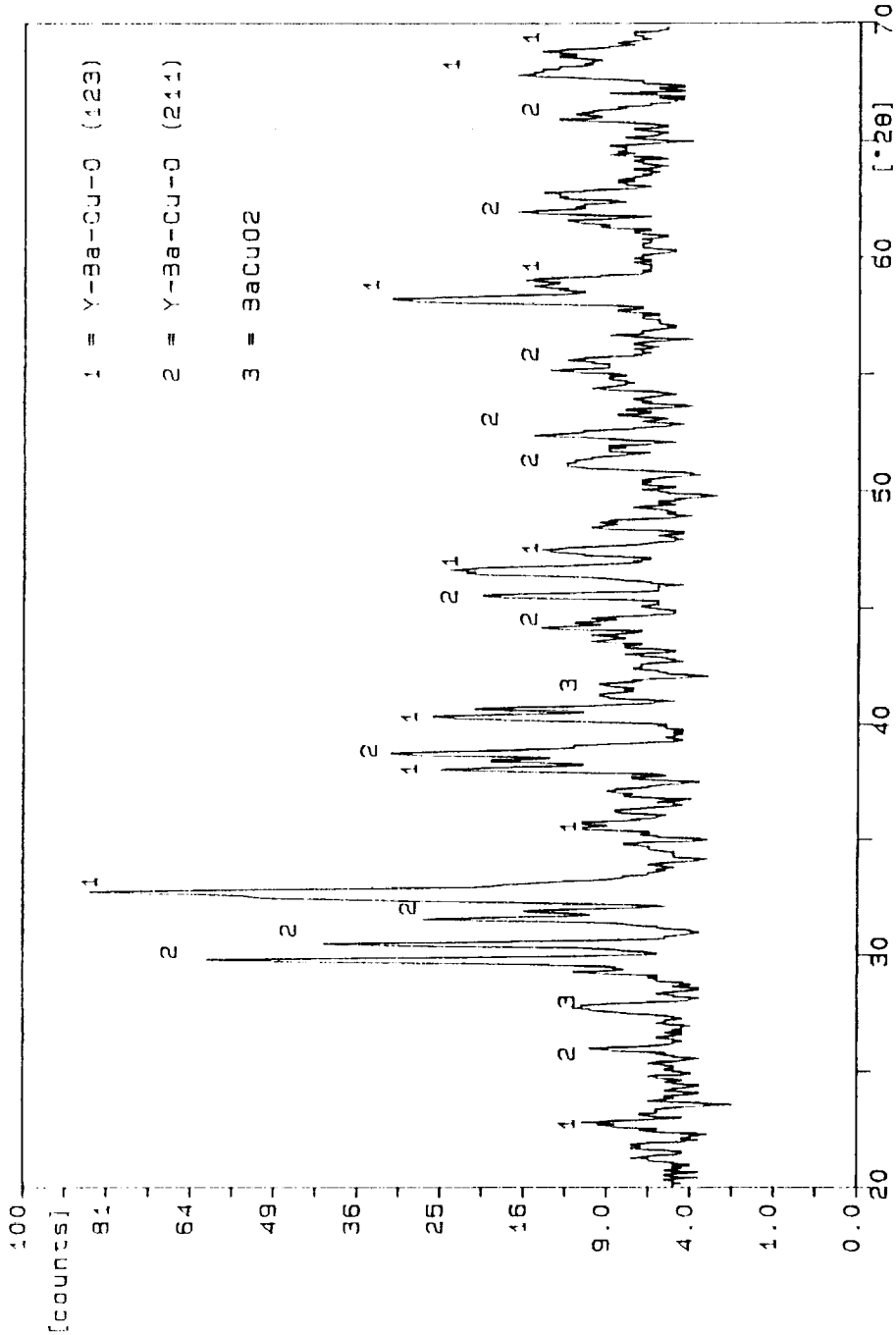

Figure 30. X-ray diffraction pattern showing the decomposition of a $YBa_2Cu_3O_{7-x}$ specimen into Y_2BaCuO_5 and $BaCuO_2$ at 945°C.

Figure 31. SEM micrograph showing the grain structure of a thermally decomposed specimen (J_c = 0 A/cm^2).

SEM micrographs showing the thermally decomposed microstructures of Ag-doped specimens fired at 935 and 945°C are shown in Figures 32 and 33 respectively. The micrograph in Figure 32 shows the precipitation of impurity phases (e.g., Y_2BaCuO_5) along the $YBa_2Cu_3O_{7-x}$ grain boundaries much like that observed in Figure 31. At 945°C, the liquid phase had begun to consume the adjacent grains and is visible between the remaining grains. Similar grain structures have been reported [43-46, 102] for materials heated well above their melting points and quenched to room temperature.

Figure 32. SEM micrograph showing the decomposition of the $YBa_2Cu_3O_{7-x}$ phase in an Ag-doped specimen fired at 935°C.

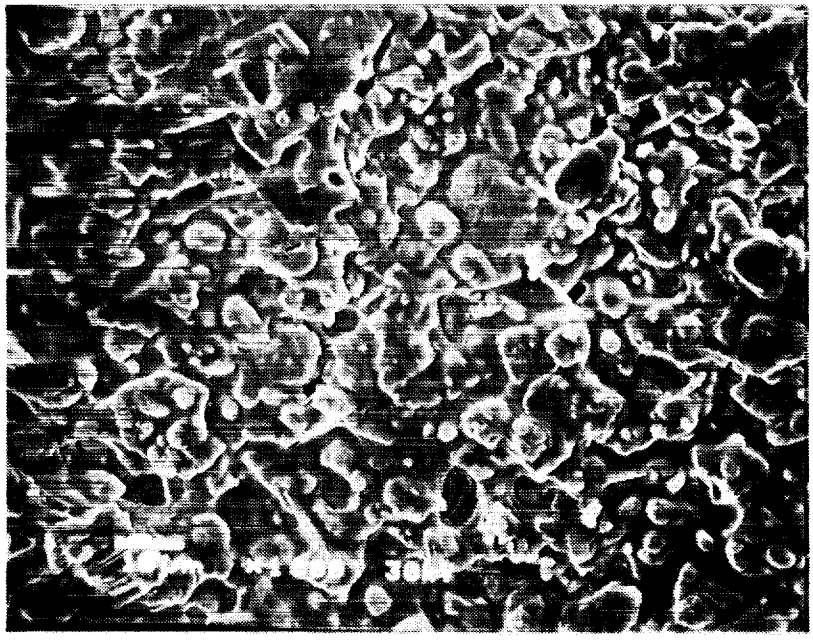

Figure 33. SEM micrograph showing the loss of crystallinity in an Ag-doped $YBa_2Cu_3O_{7-x}$ specimen fired at 945°C.

The best specimens obtained in this study were produced by combining a lower firing temperature (935°C) with a near-ideal particle size distribution (n=0.40) and avoiding silver dopants. By employing these experimental conditions, cast bodies with lower fired shrinkages (i.e., 15 volume percent) were produced. Furthermore, the microstructures obtained for these specimens showed the presence of rectangular grains typical of $YBa_2Cu_3O_{7-x}$ ceramics as indicated in the SEM micrograph shown in Figure 34.

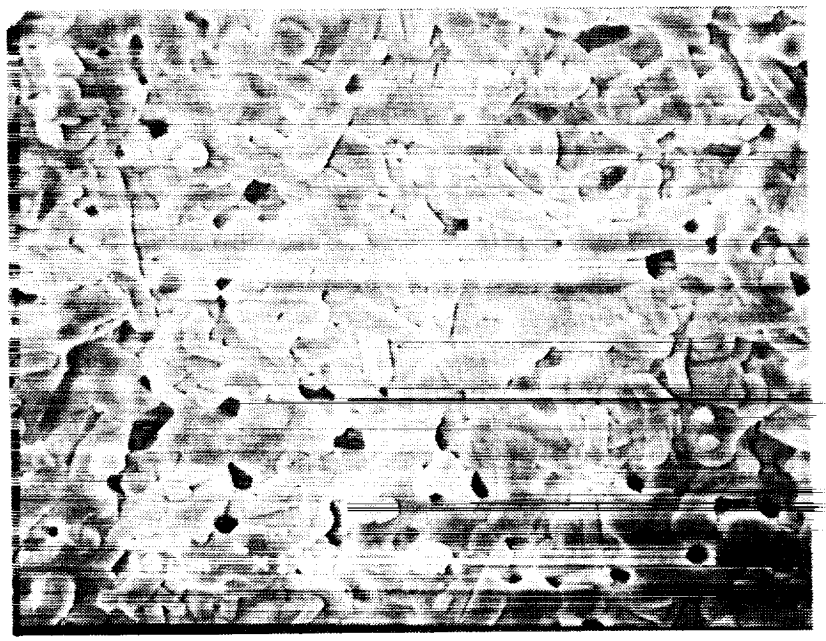

Figure 34. SEM micrograph of a specimen fired at 935°C (n = 0.40) possessing a high critical current density (Jc = 110 A/cm^2).

Additionally, cast $YBa_2Cu_3O_{7-x}$ ceramics prepared under these conditions possessed average relative densities of 90% and Jc's ranging from 75-110 A/cm^2. The average relative density and Jc of $YBa_2Cu_3O_{7-x}$ ceramics cast using powder with a

distribution modulus of n = 0.65 decreased to 80% and 10 A/cm^2 respectively for the same firing temperature. These results indicate that the fired density and critical current density may be enhanced by controlling the particle size distribution employed.

The correlation between relative density and critical current density in bulk $YBa_2Cu_3O_{7-x}$ ceramics has been reported in the literature [104-107]. The production of high quality specimens has been found to depend on densification of the powder compact below the decomposition temperature, followed by the conversion of the bulk ceramic to the superconducting phase by oxygen annealing.

Costa et al [107] reported a decrease in the critical current density of $YBa_2Cu_3O_{7-x}$ ceramics fired above 940°C due to the onset of decomposition within the superconducting phase. However, no reference to the particle size distribution within the powder compacts was made.

As evidenced by the ANOVA results in this work, the interaction between the particle size distribution and sintering temperature is significant in the processing of bulk superconductors. Although no correlation between these two variables has been previously reported for $YBa_2Cu_3O_{7-x}$ ceramics, the interaction of these parameters is routinely monitored in the manufacture of ceramics [68,90].

Additionally, all specimens doped with silver possessed significantly lower relative density and critical current density values. These low values are attributable [108-109]

to the acceleration of the thermal decomposition of the $YBa_2Cu_3O_{7-x}$ phase by the presence of Ag as previously described. Although several researchers have reported high Jc values for Ag-doped superconductive specimens [27-31], two recent studies [108-109] have shown that the use of Ag_2O as the dopant source in $YBa_2Cu_3O_{7-x}$ ceramics yields poor superconductive properties. Experimental evidence [27-31, 108-109] suggests that this effect is due to the improper distribution of the silver in the ceramic matrix.

The highest Jc values reported for Ag-doped $YBa_2Cu_3O_{7-x}$ were achieved by incorporating multiple calcining, crushing, repelletizing, and sintering treatments to effectively distribute the silver throughout the ceramic [27-31]. Conversely, the one-step conversion of Ag_2O to Ag employed in this study decreases the current density of the ceramics [108-109]. As the most effective means of enhancing the properties of $YBa_2Cu_3O_{7-x}$ ceramics through Ag additions requires several steps, the use of silver dopants is contrary to the production of net shapes.

Application of Magnetic Alignment

The objective of these experiments was to determine the applicability of magnetic grain alignment to the slip casting of superconductive powders. Magnetic fields have been found to c-axis orient $YBa_2Cu_3O_{7-x}$ grains parallel to the magnetic field while in suspension [47], making this texturing method directly applicable to some ceramic forming processes as proposed by Goretta et al [13]. In this work, the casting of

$YBa_2Cu_3O_{7-x}$ ceramics in a 0.7T magnetic field was performed, resulting in the production of c-axis oriented castings.

The microstructural analyses of the $YBa_2Cu_3O_{7-x}$ ceramics along the planes cast parallel to the applied magnetic field show a predominance of long, rectangular grains typical of c-axis orientation [47,50-51,110]. As described by Seuntjens et al [51], the microstructures of magnetically textured $YBa_2Cu_3O_{7-x}$ specimens possess a high concentration of c-axes, with some unaligned grains trapped between the aligned grains. Examples of this grain morphology are shown in Figure 35.

Although the reliability of correlating SEM images and rocking angle studies in crowded particulate systems is questionable [51], two groups have reported the degree of misalignment between c-axis oriented grains to be 15-25°[51,114]. Similar studies on individual $YBa_2Cu_3O_{7-x}$ grains aligned in epoxy matrices indicate the degree of misalignment between c axes to be approximately 3° [47]. The higher degree of misalignment in crowded particulate systems is generally attributed to particle-particle interactions during alignment and stacking faults developed as the particles come in contact with one another [51].

The c-axis orientation in slip cast $YBa_2Cu_3O_{7-x}$ was verified by X-ray diffraction of surfaces parallel to the applied magnetic field (**B** = 0.7T) and compared to data for a specimen cast under normal conditions (i.e., **B** = 0T). The presence of preferred orientation was assessed by evaluation of the relative peak intensities (I/I_o) of the (00*l*) peaks.

Figure 35. SEM micrographs showing the high quantity of long, rectangular grains typical of c-axis orientation in $YBa_2Cu_3O_{7-x}$ ceramics at 1000x (top) and 3000x (bottom).

When the c-axes are aligned, the (00*l*) planes are placed in the scattering plane, leaving the (*hk*0) peaks relatively unaffected. Thus, X-ray diffraction patterns will show the suppression of the (00*l*) peaks when a specimen is c-axis oriented [111].

As shown in Figure 36, the (003), (005), (006), and (007) peaks were suppressed by the use of magnetic alignment. The (006) peak at $2\Theta = 46.7°$ was not entirely suppressed because of the contribution of the (020) plane at the same Bragg angle. The relative peak intensities for the (00*l*) reflections in randomly oriented and c-axis aligned cast ceramics are summarized in Table 13. The X-ray diffraction data presented in Figure 36 and Table 13 are in agreement with results published in the technical literature [48,112-113].

Although the magnetic field effectively aligned the c-axes parallel to the applied field, no orientation of the current carrying ab (i.e., Cu-O) planes was observed in either the SEM or X-ray diffraction results. Additionally, no enhancement of the critical current density above the best values obtained in the previous section were observed.

As shown in Figure 37, the SEM analyses of sections cast perpendicular to the applied magnetic field revealed no preferred orientation of the grains in this direction. Additionally, the X-ray diffraction results shown in Figure 38 indicate the presence of peaks attributable to both the (*hk*0) and (00*l*) reflections.

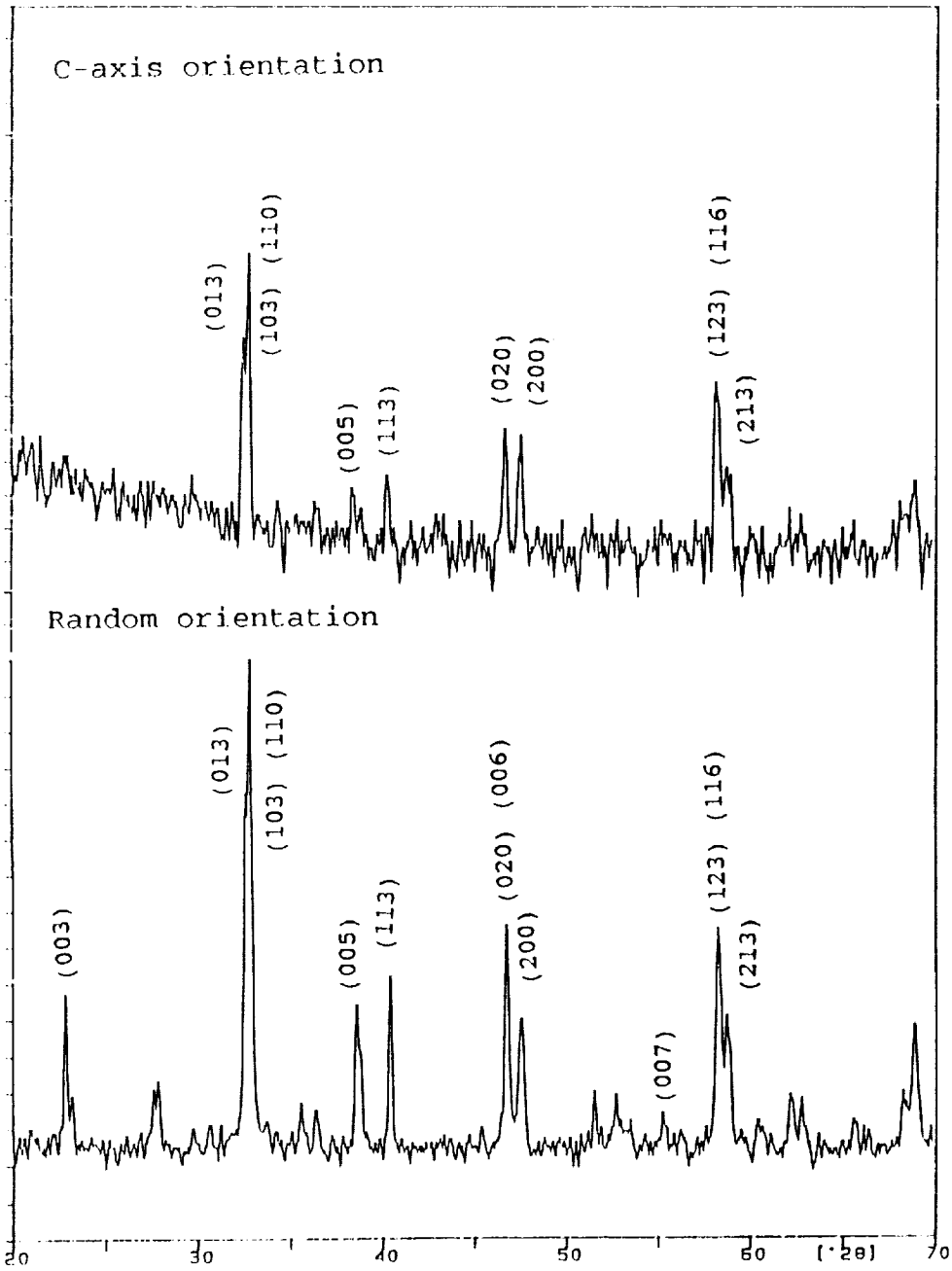

Figure 36. X-ray diffraction patterns for c-axis oriented (top) and randomly oriented (bottom) slip cast specimens.

Table 13. Comparison of (00*l*) reflections for randomly oriented (**B** = 0T) and magnetically aligned (**B** = 0.7T) grains in cast $YBa_2Cu_3O_{7-x}$.

(00*l*) Reflection	Bragg angle (2Θ)	I/I_o (**B** = 0T)	I/I_o (**B** = 0.7T))
(003)	22.9°	30	0
(005)	38.6°	30	10
(006)	46.7°	45*	30*
(007)	55.0°	10	0

*Includes contribution from (020) plane.

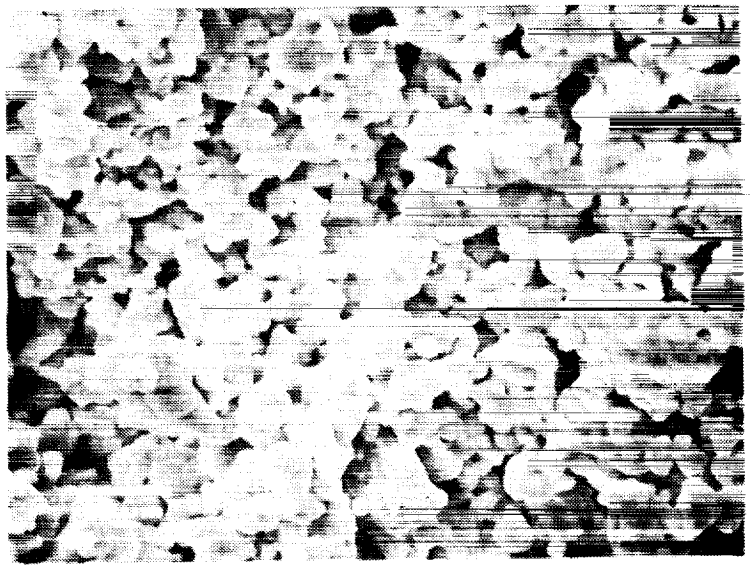

Figure 37. SEM micrograph illustrating the lack of ab orientation in planes perpendicular to the applied magnetic field in slip cast $YBa_2Cu_3O_{7-x}$.

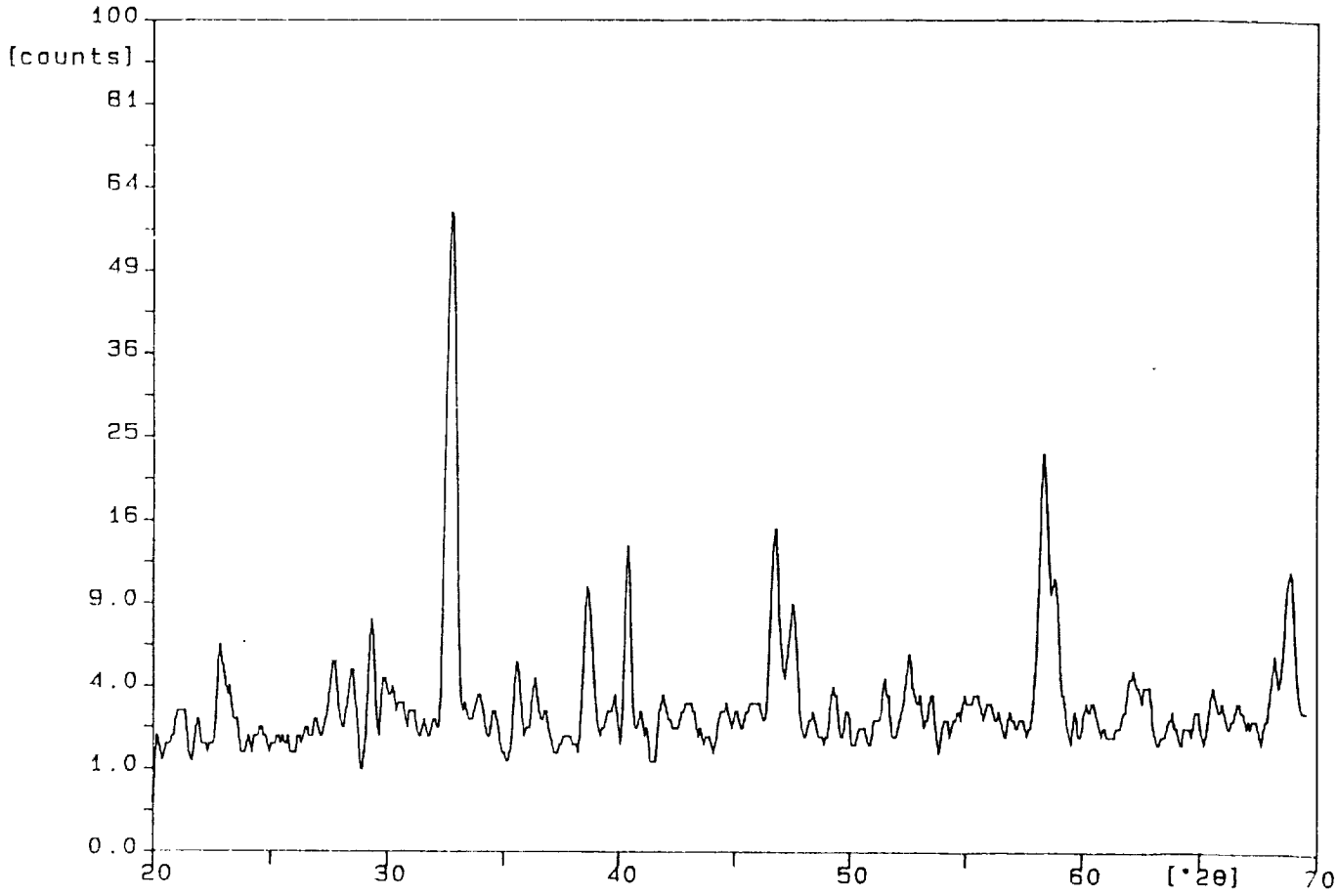

Figure 38. X-ray diffraction pattern showing the lack of preferred orientation perpendicular to the applied magnetic field.

The random orientation of the ab planes within the c-axis oriented structures is attributable to the inability of the applied magnetic field to align these planes. The application of a magnetic field unidirectionally aligns the c-axes of $YBa_2Cu_3O_{7-x}$ grains but has no effect on the current carrying ab planes [47,110]. As a result, both the SEM and X-ray diffraction results obtained for sections perpendicular to the applied magnetic field during casting closely resemble the results typically obtained for randomly oriented specimens.

These studies verified the concept [13] of combining magnetic texturing with the slip casting of $YBa_2Cu_3O_{7-x}$ ceramics. However, as the applied magnetic fields align only the c-axes, no enhancement of the critical current density was observed. This finding explains recent reports of low Jc values in magnetically textured $YBa_2Cu_3O_{7-x}$ compacts showing pronounced c-axis orientation [50,54]. In each of these reports, enhancement of the critical current density did not accompany c-axis orientation.

CONCLUSIONS

1. Steric dispersion of $YBa_2Cu_3O_{7-x}$ powders in acetone using Menhaden fish oil as a dispersant was found to be an effective combination for preparing nonaqueous slips for casting. These suspensions were found to possess a viscosity minima at 85 cps over a dispersant concentration range of 0.75 to 1.75 volume percent, providing a wide working range for slip optimization.

2. The casting of nonaqueous slips in fired ceramic molds prepared by a lost wax process yielded net-shape, $YBa_2Cu_3O_{7-x}$ ceramics with a superconductive transition temperature of 90 K.

3. The particle size distribution, sintering temperature, and the interaction of these two process parameters were found to be essential factors in controlling the slip casting of $YBa_2Cu_3O_{7-x}$ ceramics. By employing powders with near-ideal [96] particle size distributions, bulk superconductors with critical current densities ranging from 75-110 A/cm^2 were produced by firing at 935°C.

4. The performance of the casting process in the presence of a 0.7 Tesla magnetic field resulted in the production of ceramics with c-axis oriented microstructures. However, no alignment of the ab planes accompanied the orientation of the c axes. Therefore, no enhancement of the critical current density was observed. The lack of orientation of the ab planes is attributable to particle-particle interactions which occur during the forming of the ceramics [51].

RECOMMENDATIONS

1. The slip casting of $YBa_2Cu_3O_{7-x}$ powders could be performed to produce net-shape superconductors for passive magnetic systems such as bearings [61] or vibration dampers [62]

2. The use of melt-grown [39-46] $YBa_2Cu_3O_{7-x}$ powders with enhanced flux pinning properties could be performed to produce net-shape superconductors with enhanced properties. At present, the production of high levitation force materials in net shapes is difficult due to the loss of the shape during the melting process.

3. The nonaqueous casting process described in this work could also be employed to form other engineering ceramics that may be incompatible with aqueous slips.

APPENDICES

Appendix A

Chemical Suppliers

Chemical	Supplier	Location
Y_2O_3	Molycorp, Inc.	Louviers, CO
$BaCO_3$, CuO, Ag_2O, oleic acid stearic acid	Fisher Scientific	Raleigh, NC
Defloc Z3 (Menhaden fish oil)	Reichhold Chemical	Newark, NJ
Emphos PS21A	Witco Chemical Co.	New York, NY
Merpol A	E.I. Dupont de Nemours	Wilmington, DE
Aerosol OT	American Cyanamid	Wayne, NJ
Acetone Methyl ethyl ketone	Mallinckrodt	Paris, KY
Xylene	Spectrum Chemical Mfg. Corp.	Gardena, CA
Ethyl alcohol	Pharmco	Bayonne, NJ

Appendix B

Four Probe Resistance Measurement

Throughout this research, standard d.c. four probe resistance measurements [114] were performed on both $YBa_2Cu_3O_{7-x}$ and silver-doped $YBa_2Cu_3O_{7-x}$ specimens to determine the superconducting transition temperature (Tc) of the materials produced for use in the casting process.

This electrical characterization technique utilizes four electrical contacts to the test specimens. To obtain resistance versus temperature data, a known current is passed through the outer two leads while the volage drop across the inner two leads is monitored. The resistance of the sample is obtained by employing Ohm's law,

$$R = V/I \qquad (B.1)$$

where

R = electrical resistance

V = voltage across the inner two leads

I = current passed through the outer leads.

Resistance data was taken at every 0.5 K temperature interval as the sample was cooled to cryogenic conditions (~50 K).

The d.c. four probe resistance measurements were performed by the Department of Physics and Computer Science at Christopher Newport University in Newport News, VA. In this procedure, the specimens were mounted inside an APD* cryostat, and the temperature was reduced using a helium gas closed cycle refrigeration system. The temperature in the cryostat was controlled by a Lakeshore** DRC82C temperature controller,

and the resistance versus temperature data was gathered and stored using a Hewlett-Packard† 3497A data acquisition and control unit in conjunction with a Hewlett-Packard 300 series computer. A Keithly†† 220 programmable current source was employed to pass current (10mA) through the specimens, and the voltage drop across the inner two leads was measured by a Hewlett-Packard 3456A digital voltmeter.

The electrical contacts to the ceramics were made by sputtering 1500Å of gold onto the test specimens. The test specimens were partially masked during the sputtering process to produce four electrical contacts. Copper wires were then soldered to the gold contacts and connected to the appropriate instruments.

*APD Cryogenics, Inc., 1919 Vultee St., Allentown, PA.

**Lake Shore Cryotronics, Inc., 64 East Walnut St., Westerville, OH.

†Hewlitt-Packard, P.O. Box 3486, Sunnyvale, CA.

††Keithly Instruments, Inc., 28775 Aurora Rd., Cleveland, OH.

Appendix C

Critical Current Density Measurement

The critical current density [114] of each specimen was measured by employing a four probe measurement. In this procedure, current is passed through the outer two leads and the voltage across the inner two leads is monitored. The applied current density (i.e., applied current/cross sectional area) is increased until the voltage increases, indicating the loss of superconductivity. The value at which superconductivity is lost is the critical current density (A/cm^2).

The critical current density measurements were performed with the test specimens immersed in liquid nitrogen (77 K). At 77 K, the specimens exhibited zero resistance at low current values, indicated by a voltage reading of zero.

A Keithley* 220 programmable current source and a Hewlett-Packard† (HP) 3456A voltmeter were used. The applied current density was controlled by a HP 3497A data acquisition and control unit along with a 300 series HP computer. The applied current density versus voltage data was plotted on a HP 7475A Plotter as shown in Figure C.1.

*Keithly Instruments, Inc., 28775 Aurora Rd., Cleveland, OH.

†Hewlitt-Packard, P.O. Box 3486, Sunnyvale, CA.

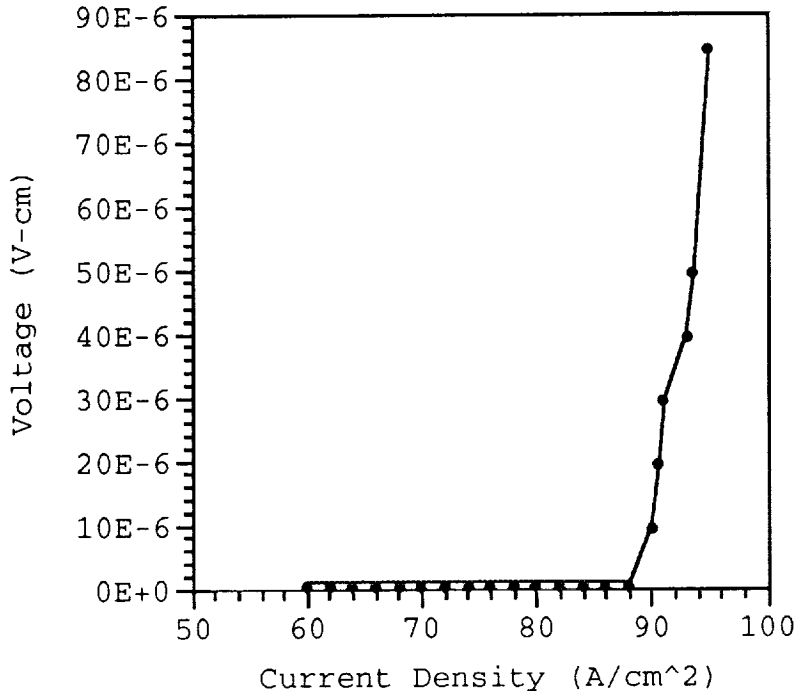

Figure C-1. Applied current density versus voltage data for specimen 16.1 (J_c = 90 A/cm^2).

Appendix D

Analysis of Variance Calculations

To determine the significance of the process variables examined in the factorial experiment, analysis of variance calculations were performed on the experimental data (relative density, porosity, and critical current density) [95]. The first step in this procedure is the calculation of a correction factor, C, using the relation,

$$C = \frac{\left(\sum Y_{i,j}\right)^2}{rt} \quad . \tag{D.1}$$

In this relation $\Sigma Y_{i,j}$ represents the sum of all of the experimental data, r is the number of replications (3), and t is the total number of treatments (16).

Next, the total sum of the squares, SS(Total), and the sum of the squares of the error term, SS(Error), were calculated as follows:

$$SS(Total) = \sum_{i,j} Y_{i,j}^2 - C \tag{D.2}$$

and

$$SS(Error) = \sum \left(Y_{i,j} - \overline{Y_i}\right)^2 \quad . \tag{D.3}$$

In equation D.3, Y_i is the average of the three experimental values at a given set of experimental conditions.

To compute the sums of squares for the primary interactions, the following relation was employed:

$$SS(A) = \frac{\sum_i (a_i)^2}{rbcd} - C \quad . \tag{D.4}$$

In this equation, a_i represents the sum of the data for the two levels of experimental condition a, and the letters b,c, and d in the denominator are the number of experimental levels of each variable tested (2).

Similarly, the sums of the squares of the first order (two-way), second order (three-way), and third order (four way) interactions were calculated by employing the following relations

$$SS(AB) = \frac{\sum_{i,j} (a_i b_j)^2}{rcd} - C - SS(A) - SS(B) \quad , \tag{D.5}$$

$$SS(ABC) = \frac{\sum_{i,j,k} (a_i b_j c_k)^2}{rd} - C - SS(A) - SS(B) - SS(C)$$

$$- SS(AB) - SS(AC) - SS(BC) \tag{D.6}$$

and

$$SS(ABCD) = \frac{\sum_{i,j,k,l}\left(a_i b_j c_k d_l\right)^2}{r} - C - SS(A) - SS(B) - SS(C) - SS(AB)$$
$$- SS(AC) - SS(BC) - SS(ABC) - SS(ABD) - SS(ACD) - SS(BCD). \quad (D.7)$$

Once the sums of the squares for each of the interactions were determined, the mean squares (MS) were calculated by dividing the sums of the squares by the degrees of freedom (df). Finally, the statistical term, F, was obtained by dividing the mean square (MS) of an experimental condition by the mean square of the error (MS Error) as shown below

$$F = MS \; / \; MS(Error) \quad (D.8)$$

The results of these calculations were then transferred to a table similar to the one shown in Table D-1. The degrees of freedom for the various treatments and interactions are given in Table D-1.

Once all of the statistical calculations were performed, the significance of each process variable and interaction was determined by comparing the calculated values of F to the critical values appearing in the F tables. If the calculated value exceeded the critical value obtained from the table, a difference is said to exist between the two experimental levels. The critical value for F at a 1 percent level of significance (i.e., $F_{1,32}$) is 7.61.

Table D-1. Analysis of variance table.

Source	df	SS	MS	F
Treatments	(abcd-1)=15			
A	(a-1)=1			
B	(b-1)=1			
C	(c-1)=1			
D	(d-1)=1			
AB	(a-1)(b-1)=1			
AC	(a-1)(c-1)=1			
AD	(a-1)(d-1)=1			
BC	(b-1)(c-1)=1			
BD	(b-1)(d-1)=1			
CD	(c-1)(d-1)=1			
ABC	(a-1)(b-1)(c-1)=1			
ABD	(a-1)(b-1)(d-1)=1			
ACD	(a-1)(c-1)(d-1)=1			
BCD	(b-1)(c-1)(d-1)=1			
ABCD	(a-1)(b-1)(c-1)(d-1)=1			
Error	abcd(r-1)=32			
Total	rabcd-1=47			

LITERATURE CITED

1. M.K. Wu, J.R. Ashburn, C.J. Torng, P.H. Hor, R.L. Meng, L. Gao, Z.J. Huang, Y.Q. Wang, and C.W. Chu, "Superconductivity at 93K in a New Mixed-phase Y-Ba-Cu-O Compound System at Ambient Pressure," *Phys. Rev. Lett.* **58** [9] 908 (1987).

2. H. Maeda, Y. Tanaka, M. Fukutomi, and T. Asano, "A New High-Tc Oxide Superconductor Without A Rare Earth Element," *Jpn. J. Appl. Phys.* **27** L209 (1988).

3. Z.Z. Sheng and A.M. Hermann, "Superconductivity in the Rare Earth Free Tl-Ba-Ca-Cu-O System above Liquid Nitrogen Temperature," *Nature* **332** 55 (1988).

4. J.H. Sharp, "A Review of the Crystal Chemistry of Mixed Oxide Superconductors," *Br. Cer. Trans. J.* **89** 1 (1990).

5. S.E. Trolier, S.D. Atkinson, P.A. Fuierer, J.H. Adair, and R.E. Newnham, "Dissolution of $YBa_2Cu_3O_{7-x}$ in Various Solvents," *Am. Cer. Soc. Bull.* **67** [4] 759 (1988).

6. L.D. Fitch and V.L. Burdick, "Water Corrosion of $YBa_2Cu_3O_{7-x}$ Superconductor," *J. Am. Cer. Soc.* **72** [10] 2020 (1989).

7. N.P. Bansal and A.L. Sandkuhl, "Chemical Durability of High Temperature Superconductor $YBa_2Cu_3O_{7-x}$ in Aqueous Environments," *Appl. Phys. Lett.* **52** 323 (1988).

8. R.L. Barns and R.A. Laudise, "Stability of Superconducting $YBa_2Cu_3O_{7-x}$ in the Presence of Water," *Appl. Phys. Lett.* **51** 1373 (1987).

9. M.F. Yan, R.L. Barns, H.M. O'Bryan, P.K. Gallagher, R.C. Sherwood, and S. Jin, "Water Interaction with the Superconducting $YBa_2Cu_3O_{7-x}$ Phase," *Appl. Phys. Lett.* **51** 532 (1987).

10. T.M. Green and M. Akinc, "Shape Forming of Superconducting Ceramics," *Bull. Am. Cer. Soc.* **70** [7] 1162 (1991).

11. S.E. Dorris, J.T. Dusek, J.J. Picciolo, H.J. Leu, J.P. Singh, A. Cazzato, and R.B. Poeppel, "Fabrication of Superconductor Coils," pp. 755-63 in Superconductivity and Ceramic Superconductors, edited by K.M. Nair and E.A. Geiss, Westerville, OH: The American Ceramic Society, Inc., 1990.

12. I. Kirschner, J. Matrai, G. Szentgyorgyi, T. Porjesz, M. Lamm, I. Molnar, G. Kovacs, P. Lukacs, T. Karman, J. Gyorgy, M Takacs, and G. Szolt, "Construction and Parameters of the First High Tc Superconducting Magnets for Small Fields," *Cryogenics* **29** 83 (1989).

13. K.C. Goretta, J.T. Dusek, J.P. singh, M.T. Lanagan, U. Balachandran, S.E. Dorris, and R.B. Poeppel, "Fabrication of Bulk Superconducting Ceramics," pp. 311-20 in World Congress on Superconductivity, edited by C.G. Burnham and R.D. Kane, Teaneck, NJ: World Scientific Publishing Co., 1988.

14. H.T. Greenaway, "The Preparation of Laboratory Ware in Magnesia by a Modification of the Slip Casting Technique," *Metallurgia* **45** 159 (1952).

15. G.M. Buck and P. Vasquez, "An Investment Ceramic Slip Casting Technique for Net-Form, Precision, Detailed Casting of Ceramic Models, Patent Pending.

16. C. Kittel, Introduction to Solid State Physics (6^{th} edition), New York: John Wiley and Sons, 1986.

17. J.S. Blakemore, Solid State Physics (2^{nd} edition), New York: Cambridge University Press, 1985.

18. K.D. Timmerhaus and T.M. Flynn, Cryogenic Process Engineering, New York: Plenum Press, 1989.

19. L.L. Hench and J.K. West, Principles of Electronic Ceramics, New York: John Wiley and Sons, 1990.

20. W. Meissner, "Magnetic Effect at the Commencement of Superconductivity," *Z. ges. Kalte-Ind.* **41** 125 (1934).

21. J. Bardeen, L.N. Cooper, and J.R. Schrieffer, "Theory of Superconductivity," *Phys. Rev.* **108** 1175 (1957).

22. L.N. Cooper, "Bound Electron Pairs in a Degenerate Fermi Gas," *Phys. Rev.* **104** 1189 (1956).

23. K.A. Muller and J.G. Bednorz, "Possible High Tc Superconductivity in the Ba-La-Cu-O System," *Z. Phys. B.* **64** 189 (1986).

24. R.J. Cava, B.Batlogg, A.P. Ramirez, D.werder, C.H. Chen, E.A. Reitman, and S.M. Zahurak, "$Ba_2YCu_3O_{7-\delta}$: Effect of Oxygen Stoichiometry, PP. 19-26 in High Temperature Superconductors, edited by M.B. Brodsky,R.C. Dynes, K. Kitazawa, and H.L. Tuller, Pittsburgh, PA: Materials Research Society (Vol. 99), 1988.

25. D.C. Larbalestier, S.E. Babcock, X. Cai, M. Daeumling, D.P. Hampshire, T.F. Kelly, L.A. Lavanier, P.J. Lee, and J. Seuntjens, "Weak Links and the Poor Transport Critical Currents of the 123 Compounds," *Physica C* **153-155** 1580 (1988).

26. D.R. Clark, T.M. Shaw, and D. Dimos, "Issues in the Processing of Cuprate Superconductors," *J. Am. Cer. Soc.* **72** [7] 1103 (1989).

27. P.N. Peters, R.C. Sisk, E.A. Urban, C.Y. Huang, and M.K. Wu, "Observation of Enhanced Properties of Silver Oxide Doped $YBa_2Cu_3O_{7-x}$," *Appl. Phys. Lett.* **52** [24] 2066 (1988).

28. V. Plechacek, V. Landa, Z. Blazek, J. Sneidr, Z. Trejbalova, and M. Cermak, "Properties of Y-Ba-Cu-O Superconductors with Ag Addition," *Physica C* **153-155** 878 (1988).

29. B. Dwir, M. Affronte, and D. Pavuna, "Critical Current and Electronic Properties of YBaCuO-Ag Compounds," pp.457-66 in Physics and Materials Science of High Temperature Superconductors, edited by R. Kossowsky, S. Methfessel, and D. Wohlleben, Boston, MA: Kluwer Academic Publishers, 1990.

30. D. Pavuna, H. Berger, J.L. Tholence, M. Affronte, R. Sanjines, A. Dubas, P. Bugnon, F. Vasey, "Electronic Properties of Superconducting $(YBa_2Cu_3O_{6.9})_{1-x}Ag_x$ Compounds," *Physica C* **153-155** 1339 (1988).

31. B. Dwir, M. Affronte, and D. Pavuna, "Evidence for Enhancement of Critical Current by Intragrain Ag in YBaCuO-Ag Ceramics," *Appl. Phys. Lett.* **55** [4] 399 (1989).

32. M.K. Malik, V.D. Nair, A.R. Biswas, R.V. Raghavan, P. Chaddah, P,K, Mishra, G.R. Kumar, and B.A. Dasannacharya, "Texture Formation and Enhanced Critical Currents in $YBa_2Cu_3O_{7-x}$," *Appl. Phys. Lett.* **52** [18] 1525 (1988).

33. S. Jin, T.H. Tiefel, R.C. Sherwood, M.E. Davis, R.B. van Dover, G.W. Kammlott, R.A. Fastnacht, and H.D. Keith, "High critical currents in Y-Ba-Cu-O Superconductors," *Appl. Phys. Lett.* **52** [24] 2074 (1988).

34. S. Jin, R.C. Sherwood, T.H. Tiefel, R.B. van Dover, G.W. Kammlott, M.E. Davis, R.A. Fastnacht, S. Nakahara, M.F. Yan, and D.W. Johnson, "Critical Current Density of the $YBa_2Cu_3O_{7-\partial}$ Superconductor as Affected by Microstructural Control," pp. 773-777 in High Temperature Superconductors, edited by M.B. Brodsky, R.C. Dynes, K. Kitazawa, and H.L. Tuller, Pittsburgh, PA: Materials Research Society (Vol. 99), 1988.

35. E.L. Venturini, D.S. Ginley, R.J. Baughman, B. Morosin, and J.F. Kwak, "Improved Magnetization for $YBa_2Cu_3O_{6.9}$ Annealed in Oxygen Above 1000°C," pp. 639-642 in High Temperature Superconductivity, edited by Brodsky, R.C. Dynes, K. Kitazawa, and H.L. Tuller, Pittsburgh, PA: Materials Research Society (Vol. 99), 1988.

36. S. Nakahara, S. Jin, R.C. Sherwood, and T.H. Tiefel, "Analysis of Dislocations in Y-Ba-Cu-O Superconductors," *Appl. Phys. Lett.* **54** [19] 1926 (1989).

37. D.S. Ginley, E.L. Venturini, J.F. Kwak, R.J. Baughman, and B. Morosin, "Improved Superconducting $YBa_2Cu_3O_{6.9}$ through High Temperature Processing," *J. Mater, Sci.* **4** [3] 496 (1989).

38. P. McGinn, W. Chen, N. Zhu, M. Lanagan, and U. Balachandran, "Microstructure and Critical Current Density of Zone Melt Textured $YBa_2Cu_3O_{6+x}$," *Appl. Phys. Lett.* **57** [14] 1455 (1990).

39. S. Kuharuangrong and J. Taylor, "Melt Processing of $YBa_2Cu_3O_{7-x}$," *J. Am. Cer. Soc.* **74** [8] 1964 (1991).

40. H. Hojaji, K.A. Michael, A. Barkatt, A.N. Thorpe, M.F. Ware, I.G. Talmy, D.A. Haught, and S. Alterscu, "A Comparative Study of Sintered and Melt-Grown Recrystallized $YBa_2Cu_3O_x$," *J. Mater. Res.* **4** [1] 28 (1989).

41. H. Hojaji, A. Barkatt, K.A. Michael, S. Hu, A.N. Thorpe, M.F. Ware, I.G. Talmy, D.A. Haught, and S. Alterscu, "Yttrium Enrichment and Improved Magnetic Properties in Partially Melted Y-Ba-Cu-O Materials," *J. Mater. Sci.* **5** [4] 721 (1990).

42. S. Everding and B. Kumar, "Preparation of $YBa_2Cu_3O_{7-x}$ High Tc Ceramic Superconductors from Melt," *J. Supercon.* **2** [2] 281 (1989).

43. M. Murakami, S. Gotoh, H. Fujimoto, K. Yamaguchi, N. Koshizuka, and S. Tanaka, "Flux Pinning and Critical Currents in Melt Processed YBaCuO Superconductors," *Supercond. Sci. Technol.* **4** 43 (1991).

44. M. Murakami, S. Gotoh, H. Fujimoto, N. Koshizuka, and S. Tanaka, "Comparative Study of Flux Pinning, Creep and Critical Currents Between YBaCuO Crystals With and Without Y_2BaCuO_5 Inclusions," pp. 241-248 in AMSAHTS '90, edited by L.H. Bennett, Y. Flom, and K. Moorjani, NASA Conference Publication 3100, 1991.

45. M. Murakami, M. Morita, and N. Koyama, "Magnetization of a $YBa_2Cu_3O_7$ Crystal Prepared by the Quench and Melt Growth Process," *Jap. J. Appl. Phys.* **28** [7] L1125 (1989).

46. W.H. Chen, N. Zhu, and P.J. McGinn, "Observation of Attractive Forces in Zone-Melted $YBa_2Cu_3O_{7-x}$," *Mater. Lett.* **9** [5,6] 189 (1990).

47. D.E. Farrell, B.S. Chandrasekhar, M.R. DeGuire, M.M. Fang, V.G. Kogan, J.R. Clem, and D.K. Finnemore, "Superconducting Properties of Aligned Crystalline Grains of $YBa_2Cu_3O_{7-\partial}$, *Phys. Rev. B* **36** [7] 4025 (1987).

48. R.H. Arendt, A.R. Gaddipati. M.F. Garbauskas, E.L. Hall, H.R. Hart, K.W. Lay, J.D. Livingston, F.E. Luborsky and L.L. Schilling, "Aligned Sintered Compacts of $RBa_2Cu_3O_{7-x}$ (R=Dy, Er, Eu, Gd, Ho, Y)," pp. 203-208 in High Temperature Superconductors, edited by M.B. Brodsky, R.C. Dynes, K. Kitazawa, and H.L. Tuller, Pittsburgh, PA: Materials Research Society (Vol. 99), 1988.

49. B.A. Glowacki and J.E. Evetts, "Critical Current Anisotropy in Sintered Superconducting $YBa_2Cu_3O_7$, pp. 419-22 in High Temperature Superconductors, edited by M.B. Brodsky, R.C. Dynes, K. Kitazawa, and H.L. Tuller, Pittsburgh, PA: Materials Research Society (Vol. 99), 1988.

50. Y. Nakagawa, H. Noda, A. Yoneda, and K. Sakata, "Superconducting Properties of Grain-Oriented Samples of $YBa_2Cu_3O_y$," *Jap. J. Appl. Phys.* **28** [4] L547 (1989).

51. J. Seuntjens, X. Cai, and D.C. Larbalestier, "Preparation and Characterization of Magnetically Textured Y and Dy 123 Compounds," *IEEE Trans. Magnetics* **25** [2] 2021 (1989).

52. K. Chen, B. Mahewswaran, Y.P. Liu, B.C. Giessen, C. Chan, and R.S. Markiewicz, "Critical Current Enhancement in Field-Oriented $YBa_2Cu_3O_{7-\partial}$, *Appl. Phys. Lett.* **55** [3] 289 (1989).

53. G. Oszlanyi, G. Faigel, S. Pekker, A. Janossy, "Orientation Distribution of Magnetic Field Oriented $YBa_2Cu_3O_6$ Powders," *Physica C* **167** 157 (1990).

54. J.E. Tkaczyk, K.W. Lay, and H.R. Hart, "Anisotropic Critical Currents in Aligned Sintered Compacts of $YBa_2Cu_3O_{7-\partial}$," pp. 557-65 in Superconductivity and Applications, edited by H.S. Kwok, Y.H. Kao, and D.T. Shaw, New York: Plenum Press, 1990.

55. R.S. Markiewicz, K. Chen, B. Maheswaran, Y.P. Liu, B.C. Giessen, and C. Chan, "$YBa_2Cu_3O_{7-\partial}$: Enhancing Jc by Field Orientation," pp. 567-72 in Superconductivity and Applications, edited by H.S. Kwok, Y.H. Kao, and D.T. Shaw, New York: Plenum Press, 1990.

56. G. Walker, W. Ellison, and S. Zylstra, "Cryocoolers for the New High Temperature Superconductors," pp. 252-72 in World Congress on Superconductivity, edited by C.G. Burnham and R.D. Kane, Teaneck, NJ: World Scientific Publishing Co., 1988.

57. R.R. Romanofsky and M.M. Sokoloski, "Prospects and Progress of High Tc Superconductivity for Space Applications," pp. 477-486 in AMSAHTS '90, edited by L.H. Bennett, Y. Flom, and K. Moorjani, NASA Conference Publication 3100, 1991.

58. K. Krishen and A. Ignatiev, "Future Superconductivity Applications In Space - A Review," pp. 141-154 in World Congress on Superconductivity, edited by C.G. Burnham and R.D. Kane, Teaneck, NJ: World Scientific Publishing Co., 1988.

59. R. Simon, "High Tc Thin Films and Electronic Applications," *Physics Today* **44** [6] 64 (1991).

60. C.F. Lewis, "Cool Applications for High-Temp Superconductors," *Mater. Engr.* **108** [2] 17 (1991).

61. B.R. Weinberger, L. Lynds, and J.R. Hull, "Magnetic Bearings Using High-Temperature Superconductors: Some Practical Considerations," *Supercon. Sci. Technol.* **3** 381-88 (1990).

62. D. Rao, "Evaluation of Performance Characteristics of Superconducting Bearings and Dampers," Phase II Final Report, Contract Number SDIO-84-89-C-0043, Dec. 23, 1991.

63. J.C. Macfarlane, R. Driver, R.B. Roberts, and E.C. Horrigan, "Electromagnetic Shielding Properties of Yttrium Barium Cuprate Superconductor," *Cryogenics* **28** 303 (1988).

64. Leskala, J.K. Truman, C.H. Mueller, and P.H. Holloway, "Preparation of Superconducting Y-Ba-Cu-O Thin Films," *J. Vac. Sci. Technol.* **7** [6] 3147 (1989).

65. N.P. Bansal, R.N. Simons, and D.E. Farrell, "High Tc Screen-Printed $YBa_2Cu_3O_{7-x}$ Films: Effect of the Substrate Material," *Appl. Phys. Lett.* **53** [7] 603 (1988).

66. M. Sacchi, F. Sirotti, B. Morten, M. Prudenziati, "High Tc Superconductivity in Y-Ba-Cu-O Screen-Printed Films, *Appl. Phys. Lett.* **53** [12] 1110 (1988).

67. D.E. Bloomberg, D.S. Applegate, T.L. Tolt, M.T. Lanagan, J.T. Dusek, R.B. Poeppel, and K.C. Goretta, "Slip Casting High-Tc Superconductors," *J. Mater. Sci.* **8** 759 (1989).

68. J.S. Reed, Introduction to the Principles of Ceramic Processing, pp. 380-394, New York: John Wiley and Sons, 1988.

69. D.S. Adcock and I.C. McDowall, "The Mechanism of Filter Pressing and Slip Casting," *J. Am. Cer. Soc.* **40** [10] 355 (1957).

70. F. Singer and S.S. Singer, Industrial Ceramics,pp. 754-776, New York: Chemical Publishing Co., Inc., 1963.

71. P.D.S. St. Pierre, "Slip Casting NonClay Ceramics," pp. 45-51 in Ceramic Fabrication Processes, edited by W.D. Kingery, New York: John Wiley and Sons, 1958.

72. D.J. Shaw, Introduction to Colloid and Surface Chemistry (3rd edition), pp. 208-211, Boston: Butterworth & Co., 1980.

73. M.J. Rosen, Surfactants and Interfacial Phenomena (2nd edition), pp. 359-360, New York: John Wiley and Sons, 1989.

74. T.F. Tadros, "Suspensions," pp. 197-220 in Surfactants, edited by T.F. Tadros, Orlando, FL: Academic Press Inc., 1984.

75. R.D. Nelson, Dispersing Powders in Liquids, pp. 41-42, New York: Elsevier, 1988.

76. W.B. Russell, D.A. Saville, and W.R. Schowalter, Colloidal Dispersions, pp. 310-328, New York: Cambridge University Press, 1989.

77. G.D. Parfitt and J. Peacock, "Stability of Colloidal Dispersions in Nonaqueous Media," pp. 163-226 in Surface and Colloid Science (Volume 10), edited by E. Matijevic, New York: Plenum Press, 1978.

78. D.W.J. Osmond and F.A. Waite, "The Theoretical Basis for the Steric Stabilization of Polymer Dispersions Prepared in Organic Media," pp. 9-44 in Dispersion Polymerization in Organic Media, edited by K.E.J. Barrett, New York: John Wiley and Sons, 1975.

79. CRC Handbook of Chemistry and Physics (66th edition), pp. C385 edited by R.C. Weast, M.J. Astle, and W.H. Beyer, Boca Raton, FL: Chemical Rubber Company Press, Inc., 1985.

80. D.N.L. McGown, G.D. Parfitt, and E. Willis, "Stability of Non-Aqueous Dispersions: I. The Relationship between Surface Potential and Stability in Hydrocarbon Media," *J. Colloid. Sci.* **20** 650-64 (1965).

81. H. Koelmans and J.T.H. Overbeek, "Stability and Electrophoretic Deposition of Suspensions in Nonaqueous Media," *Discuss. Faraday Soc.* **18** 52 (1954).

82. P.D. Calvert, E.S. Tormey, and R.L. Pober, "Fish Oil and Triglycerides as Dispersants for Alumina," *Am. Cer. Soc. Bull.* **65** [4] 669 (1986).

83. M.V. Parish, R.R. Garcia, and H.K. Bowen, "Dispersions of Oxide Powders in Organic Liquids," *J. Mater. Sci.* **20** 996 (1986).

84. V.R. Damerell, K. Gayer, and H. Laudenslager, "Effect of Surface-Active Agents upon Dispersions of Silica in Xylene," *J. Phys. Chem.* **49** 436 (1945).

85. D.N.L. McGown and G.D. Parfitt, "Stability of Non-Aqueous Dispersions," *Disc. Faraday Soc.* **42** 225 (1966).

86. K. Mikeska and W.R. Cannon, "Dispersants for Tape Casting Pure Barium Titanate," pp. 164-83 in Forming of Ceramics, edited by J.A. Maugles, Columbus, OH: The American Ceramic Society, Inc., 1984.

87. V.R. Damerell and A. Urbanic, "A Study of the Colloidal System Carbon Dispersed in Xylene," *J. Phys. Chem.* **48** 125 (1944).

88. V.R. Damerell and R. Mattson, "Effect of Surface-Active Agents upon Dispersions of Calcium Carbonate in Xylene," *J. Phys. Chem.* **48** 134 (1944).

89. F.M. Fowkes "Mechanism of Electric Charging Particles in Nonaqueous Liquids," Reprinted from ASC Symposium Series, No. 200, 1982.

90. G.W. Phelps and M.G. McLaren, "Particle-Size Distribution and Slip Properties," pp. 211-225 in Ceramic Processing before Firing, edited by G.Y. Onoda and L.L. Hench, New York: John Wiley and Sons, 1978.

91. A.H.M. Andreason, "The Relation of Fineness to Physical Requirements," *J. Soc. Glass. Technol.* **24** 166 (1940).

92. J.E. Funk and D.R. Dinger, "Slip Control Using Particle-Size Analysis and Specific Surface Area," *Am. Cer. Soc. Bull.* **67** 890 (1988).

93. R.J. Cava, B. Batlogg, R.B. van Dover, D.W. Murphy, S. Sunshine, T. Siegrist, J.P. Rietman, S. Zahurak, and G.P. Espinosa, "Bulk Superconductivity at 91K in Single-Phase Oxygen-Deficient Perovskite $YBa_2Cu_3O_{9-\delta}$," *Phys. Rev. Lett.* **58** 1676 (1987).

94. S. Lowell and J.E. Shields, Powder Surface Area and Porosity, 2nd edition, pp. 217-218, New York: Chapman and Hall, 1984.

95. R.G.D. Steel and J.H. Torrie, Principles and Procedures of Statistics: A Biometral Approach, 2nd edition, pp. 336-376, New York: McGraw-Hill Book Company, 1980.

96. J.T. Jones and M.F. Bernard, Ceramics: Industrial Processing and Testing, pp. 107-109, Ames, Iowa: The Iowa State University Press, 1972.

97. N.M. Alford, T.W. Button, and J.D. Birchall, "Processing Properties and Devices in High Tc Superconductors, *Supercond. Sci. Technol.* **3** 1 (1990).

98. R.K. Bordia, H.S. Horowitz, M.A. subramanian, J.B. Michel, E.M. McCarron, C.C. Toradi, J.D. Bolt, U. Chowndhry, E. Lopdrup, and S.J. Poon, "Sintering and Microstructure - Property Relations For $YBa_2Cu_3O_{7-x}$," pp. 245-48 in High Temperature Superconductors, edited by M.B. Brodsky, R.C. Dynes, K. Kitazawa, and H.L. Tuller, Pittsburgh, PA: Materials Research Society (Vol. 99), 1988.

99. K. Gotoh, H. Enomoto, K. Iida, Y. Tanaka, N. Mori, H. Ozaki, "Effect of Thermal Processing on the Microstructures and Superconducting Properties of $YBa_2Cu_3O_{7-x}$," pp. 265-68 in High Temperature Superconductors, edited by M.B. Brodsky, R.C. Dynes, K. Kitazawa, and H.L. Tuller, Pittsburgh, PA: Materials Research Society (Vol. 99), 1988.

100. A. Doroszkowski and R. Lambourne, "Effect of Molecular Architecture of Long Chain Fatty Acids on the Dispersion of Titanium Dioxide in Non-aqueous Liquids,' *Disc. Faraday Soc.* **65** 252 (1978).

101. S. Jin, T.H. Tiefel, R.C. Sherwood, R.B. van Dover, M.E. Davis, G.W. Kammlott, and R.A. Fastnacht, "Melt-Textured Growth of Polycrystalline $YBa_2Cu_3O_{7-x}$ With High Transport Jc at 77 K," *Phys. Rev. B* **37** 7850 (1988).

102. W.D. Kingery, H.K. Bowen, and D.R. Uhlmann, *Introduction to Ceramics*, 2nd edition, p. 499, New York: John Wiley and Sons, 1976.

103. M.A. Rodriguez, R.L. Snyder, B.J. Chen, D.P. Matheis, S.T. Misture, V.D. Frechette, G. Zorn, H.E. Gobel, and B. Seebacher, "The High-Temperature Reactions of $YBa_2Cu_3O_{7-x}$," *Physica C* **206** 43-50 (1993).

104. N.M. Alford, C.J. Clegg, M.A. Harmer, J.D. Birchall, K. Kendall, and D.H. Jones, "The Effect of Density on Critical Current and Oxygen Stoichiometry of $YBa_2Cu_3O_x$ Superconductors," *Nature* **332** 58 (1988).

105. N.M Alford, J.D. Birchall, W.J. Clegg, and K. Kendall, "Critical Currents of Sintered and Melt-Textured $YBa_2Cu_3O_x$," *J. Appl. Phys.* **65** 2856(1989).

106. C.W. Cheng, A.C. Rose-Innes, N.M. Alford, M.A. Harmer, and J.D. Birchall, "The Effect of Porosity on the Superconducting Properties of $YBa_2Cu_3O_x$ Ceramic," *Supercond. Sci. Tech.* **1** 113 (1988).

107. F.M. Costa, A.P. Goncalves, M.L. Almeida, and J.M. Vieira, "Grain Connectivity and Superconductivity of Bulk High Temperature Superconductors," pp. 519-526, in Physics and Materials Science of High Temperature Superconductors, edited by R. Kossowsky S. Methfessel, and D. Wohlleben, Boston, MA: Kluwer Academic Publishers, 1990.

108. T.H. Tiefel, S. Jin, R.C. Sherwood, M.E. Davis, G.W. Kammlott, P.K. Gallagher, D.W. Johnson, R.A. Fastnacht, and W.W. Rhodes, "Grain-Growth Enhancement In the $YBa_2Cu_3O_{7-\partial}$ Superconductor By Silver Doping," *Mater. Lett.* **7** 363 (1989).

109. J.M. Seuntjens and D.C. Larbalestier, "On the Improvement of $DyBa_2Cu_3O_{7-\partial}$ Properties Through Better Sintering," *J. Appl. Phys.* **67** 2007 (1990).

110. M. Wacenovsky, H.W. Weber, O.B. Hyun, D.K. Finnemore, and K. Mereiter, "Magnetization and Susceptibility of Grain-Aligned $HoBa_2Cu_3O_{7-x}$ Superconductors," *Physica C* **160** 55 (1989).

111. J.M. Tranquada, A.I. Goldman, A.R. Moodenbaugh, G. Shirane, S.K. Sinha, A.J. Jacobson, J.T. Lewandowski, "Observation of Alignment of Superconducting Particles in a Magnetic Field Using Neutron Diffraction," *Phys. Rev. B* **37** [1] 519 (1988).

112. S.A. Solin, N. Garcia, S. Vieira, and M. Hortal, "X-ray Studies of Field-Induced Orientation of Small Superconducting Particles," *Physica C* **153-155** 986 (1988).

113. S.C. Peterson and H.J. Cima, "Magnetic Inducement of Texture in $Ba_2YCu_3O_{7-x}$ Particle Assemblies Under Cryogenic Conditions," *J. Am. Cer. Soc.* **71** [11] C458 (1988).

114. J.D. Doss, Engineer's Guide to High Temperature Superconductivity, pp. 56-69, New York: John Wiley and Son 1989.

REPORT DOCUMENTATION PAGE

Form Approved
OMB No. 0704-0188

1. AGENCY USE ONLY (Leave blank)	2. REPORT DATE	3. REPORT TYPE AND DATES COVERED
	March 1994	Contractor Report

4. TITLE AND SUBTITLE

Nonaqueous Slip Casting of $YBa_2Cu_3O_{7-x}$ Superconductive Ceramics

5. FUNDING NUMBERS

NGT-50548

142-20-14-02

6. AUTHOR(S)

Matthew W. Hooker and Theodore D. Taylor

7. PERFORMING ORGANIZATION NAME(S) AND ADDRESS(ES)

Clemson University
Dept. of Ceramic Engineering
Clemson, SC 29634-0907

8. PERFORMING ORGANIZATION REPORT NUMBER

9. SPONSORING/MONITORING AGENCY NAME(S) AND ADDRESS(ES)

NASA Langley Research Center
Hampton, VA 23681-0001

10. SPONSORING/MONITORING AGENCY REPORT NUMBER

NASA CR-4575

11. SUPPLEMENTARY NOTES

Submitted in partial fulfillment of the requirements for the degree of Doctor of Philosophy in Ceramic Engineering from Clemson University, August 1993.

12a. DISTRIBUTION/AVAILABILITY STATEMENT

Unclassified - Unlimited
Subject Category 76

12b. DISTRIBUTION CODE

13. ABSTRACT *(Maximum 200 words)*

This study investigates the slip casting of $YBa_2Cu_3O_{7-x}$ powders using nonaqueous carrier liquids and fired ceramic molds. The parameters of the process examined here include (1) the rheological properties of $YBa_2Cu_3O_{7-x}$ powder dispersed in various solvent/dispersant systems, (2) the combination of nonaqueous slips with fired ceramic molds to form the superconductive ceramics, (3) the process-property relationships using a four-factor factorial experiment, and (4) the applicability of magnetic fields to align the $YBa_2Cu_3O_{7-x}$ grains during the casting process.

14. SUBJECT TERMS

High temperature superconductors, forming, slip casting

15. NUMBER OF PAGES
116

16. PRICE CODE
A06

17. SECURITY CLASSIFICATION OF REPORT	18. SECURITY CLASSIFICATION OF THIS PAGE	19. SECURITY CLASSIFICATION OF ABSTRACT	20. LIMITATION OF ABSTRACT
Unclassified	Unclassified	Unclassified	